



Linnæus University

Analysis of bending stiffness of composite timber-glass beams



Authors: Bardia Tamizkar
Supervisor LNU: Michael Dorn
Examiner, LNU: Björn Johannesson

Course Code: 5BY31E

Semester: Spring 2022 30 credits

*Linnæus University, Faculty of Technology
Department of Building Technology*

Abstract

Engineers and architects have always been looking for new ways to remove the bound between structures and nature which led to the usage of glass and wood combinations as a structural member in glass ceilings, walls, or balconies. The combination of glass and wood has always been used as a non-load bearing member or for its design purposes in the past. Glass is primarily used as windows currently, but today, due to the improvement of technology and the need for new elements, it is used in different combinations such as timber-glass composites and Translucent Concrete elements.

Due to the fact that wood solely can be used as a structural member in buildings, and relying on the acceptable physical properties of wood, it can be used in modern and tall buildings and structures. In modern structures, glass is also used for optimal use of space and communication with the exterior of the building.

Does the combination of these two materials and the construction of roofs or columns and composite beams have sufficient load-bearing capacity and are stiff enough?

In this thesis, the possibilities and limitations of new materials in beams are examined to create a more sustainable design both in the interior design and the structural value of a building. A combination of wood and glass in composite beams will be examined to define their load-bearing capacity and bending strength through-loading tests. The results will be compared with FEM simulations using Abaqus software and beam simulation to be able to provide good results for this combination.

Keywords: Timber, Glass, Composite beams, Bending stiffness, four-point load experimental test, Simulation, Abaqus.

Acknowledgments

This thesis is the last chapter of my studies in the master's program in Sustainable Structural engineering at Linnaeus University, Växjö, Sweden.

I would like to thank Linnaeus University and the Department of Building Technology for giving me this opportunity to expand my profession and for leading me towards a new chapter in my life and professional career.

I would like to give my greatest gratitude to my supervisor, Michael Dorn, for his amazing supervision and insightful feedback. I am extremely grateful for his guidance and creative methodology for leading me patiently through this thesis.

Finally, I would also like to deeply thank my family for their continuous support and especially my wife for her love, sacrifices and understanding during my studies. Without them, I would not have been able to proceed with this study to reach my goals.

Bardia Tamizkar

Växjö, 10st of April 2023

Table of Contents

ABSTRACT	II
ACKNOWLEDGMENTS	IV
LIST OF FIGURES	VIII
LIST OF TABLES	X
1. INTRODUCTION	1
1.1 BACKGROUND AND PROBLEM DESCRIPTION.....	1
1.2 LITERATURE REVIEW.....	3
1.3 AIM AND PURPOSE.....	5
1.4 HYPOTHESIS AND LIMITATIONS.....	5
2. MATERIAL AND METHODS	7
2.1 MATERIAL PROPERTIES.....	8
2.1.1 Glass.....	8
2.1.2 PVB film.....	10
2.1.3 Wood.....	11
2.1.4 Adhesive.....	12
2.2 CALCULATION OF BEAM BENDING STIFFNESS.....	13
3. EXPERIMENTAL TESTING	17
3.1 TEST SET-UP.....	17
3.1.1 Beam group 1 (float-float).....	22
3.1.2 Beam group 2 (heat-strengthened -float).....	25
3.1.3 Beam group 3 (strengthened-strengthened).....	28
3.3 RESULTS AND EVALUATION.....	31
4. ANALYTICAL SOLUTION	33
4.1 ANALYTICAL METHOD.....	33
4.2 ANALYTICAL RESULTS.....	36
5. SIMULATION IN ABAQUS	37
5.1 INTRODUCTION.....	37
5.2 MODELLING.....	37
5.3 MATERIAL DEFINITION.....	38
5.4 MESH AND SUPPORTS.....	39
5.5 RESULTS.....	40
6. ANALYSIS	43
6.1 LOAD-BEARING CAPACITY.....	43
6.2 BENDING STIFFNESS COMPARISON.....	44
7. CONCLUSIONS	45
APPENDIX	47

REFERENCES..... LI

List of figures

Figure 1: Exterior view of Fallingwater (Frank Lloyd Wright, 1935).....	2
Figure 2: Cross section of composite glass-timber beam.	7
Figure 3: Examples of three types of glass.	9
Figure 4: Measurement and loading position of composite beam.	14
Figure 5: Four-point bending test setup of the timber–glass composite beam, including the loading system and displacement sensors.	18
Figure 6: The nine tested composite timber–glass I-shaped beam specimens.....	19
Figure 7: Cross-section and dimension of the timber–glass I-shaped beam.....	19
Figure 8: Strain gauge locations at the midspan of the timber–glass composite beam: (1) top of the upper timber flange – flange tension zone, (2) below the upper flange – flange compression zone, (3) upper side of the glass web – glass tension zone, and (4) lower side of the glass web – glass compression zone.	20
Figure 9: Load test machine used for four-point bending tests. The yellow arrows indicate the locations of the two symmetrically applied point loads on the beam.	21
Figure 10: Setup of displacement sensor for local displacement measurement (top of beam).....	21
Figure 11: Setup of displacement sensor for global displacement measurement (bottom of beam).....	22
Figure 12: Crack development in the glass web near the load application points, located in the shear-dominated region between the supports and the point loads.	23
Figure 13: Overall view of the beam after failure showing the final crack distribution and the beam configuration at failure.	23
Figure 14: Applied load–global displacement curves for double-layer float glass beams, where the global displacement represents the midspan displacement of the beam.	24
Figure 15: Applied load–local displacement curves for double-layer float glass beams, where the local displacement represents the displacement measured between the support and the load point.....	24
Figure 16: Crack formation in the tested beam.....	25
Figure 17: Crack formation in the tested beam showing different perspectives of the same specimen.	26
Figure 18: Beams standing after failure of the beams with one-layer float glass and one-layer heat-strength glass.....	26
Figure 19: Applied load–global displacement curves for beams with one-layer float glass and one-layer heat-strengthened glass, where the global displacement represents the midspan displacement of the beam.	27

Figure 20: Applied load–local displacement curves for beams with one-layer float glass and one-layer heat-strengthened glass, where the local displacement represents the displacement measured between the support and the load point. .	27
Figure 21: Crack patterns of beams with double-layer heat-strengthened glass.	28
Figure 22: Beams standing after failure of double-layer heat-strengthened glass beams.	29
Figure 23: Applied load–global displacement curves for double-layer heat-strengthened glass beams, where the global displacement represents the midspan displacement of the beam.....	29
Figure 24: Applied load–local displacement curves for double-layer heat-strengthened glass beams, where the local displacement represents the displacement measured between the support and the load point.	30
Figure 25: Cross-section and geometric properties of the composite timber-glass beam.	33
Figure 26: Model configuration and boundary conditions.	38
Figure 27: Deformed shape of the simulated half beam (deformation visually scaled for clarity).	40
Figure 28: Measurement positions and support condition used in the Abaqus model.....	41
Figure 29: Load-time and time-global displacement diagram.	47
Figure 30: Load-time and time-local displacement diagram.	48
Figure 31: Bending stiffness diagram from global displacement.	49
Figure 32: Bending stiffness diagram from local displacement.	50

List of tables

Table 1: Mechanical properties of annealed float glass and heat-strengthened glass (adapted from Hamm [2] and Cruz & Pequeno [9]).	10
Table 2: Mechanical properties of PVB film (adapted from [21, 22]).	10
Table 3: Characteristic and mechanical properties of Kerto-S LVL (adapted from [25]).	12
Table 4: Characteristic properties of SikaSil SG500 (adapted from [29] and manufacturer's technical data sheet).	13
Table 5: Calculation of bending stiffness (EI) based on load-point, local, and global displacement measurements in four-point bending.	16
Table 6: Geometry of glass-timber composite beams.	20
Table 7: Results of the beams with double float-glass.	25
Table 8: Results of the beam with one-layer float and one-layer heat-strength glass.	28
Table 9: Results of the beam with double heat-strength glass.	30
Table 10: Calculated bending stiffness of each group.	32
Table 11: Material properties used for the LVL Kerto wood in the Abaqus simulation.	38
Table 12: Material properties used in the Abaqus simulation.	39
Table 13: Results from Abaqus.	41
Table 14: Comparison of maximum tensile stress in the composite beam.	41
Table 15: Calculated bending stiffness values from Abaqus simulation results using the four-point bending relationships.	42
Table 16: Comparison results from experimental test, Abaqus and analytical solution.	43
Table 17: Comparison results from experimental test and Abaqus.	44

1. Introduction

Steel and concrete are the most common materials used in modern load-bearing structures. However, the use of wood as one of the traditional materials in the construction industry is expanding. With the improvement of different technologies and science, wood is being used more and more. Wood is one of the best natural and sustainable materials used with considerable excellent strength and stiffness in compression. It is flexible in design and hence it is a good material for different parts of the construction because of its lightness and its harmony with nature.

Additionally, wood combines easily with other materials and at the same time maintains its physical properties. One of these materials is glass which can be combined with wood and create a strong combination for structures. One of the advantages of using this composite is its lightness and transparency. In this research, composite beams of glass and wood will be examined to obtain the bending stiffness of the beams using an experimental test regime and simulations with a finite element program.

1.1 Background and problem description

Traditionally, glass has been used mainly in façades and interior partitions. In recent years, however, researchers and engineers have increasingly explored its potential for structural applications, as noted by Klos and Bedon [1]. Studies have shown that combining glass with timber can significantly enhance its performance, particularly under loading or impact conditions, as demonstrated by Hamm [2]. Timber helps reduce the brittleness of glass and provides flexibility, as it can be easily shaped and adapted for various structural configurations. Depending on the design, timber can function as either a primary load-bearing element or a secondary structural support.

The performance of glass and timber both individually and as a composite depends on many factors, such as load distribution, connection details, and environmental influences. Understanding the interaction between these two materials is essential for optimizing their use in modern architecture and structural design.

Architects and engineers have long sought ways to bring nature and structure closer together, especially in organic architecture. A notable example is the Waterfall House, designed by Frank Lloyd Wright in 1935, see Figure 1. His goal was to create harmony between buildings and their natural surroundings. He believed that people thrive in spaces connected to nature. His designs emphasized borderless interiors, transparency, and openness ideas that continue to inspire today's timber-glass structures.



Figure 1: Exterior view of Fallingwater (Frank Lloyd Wright, 1935).

Wright's architectural philosophy, particularly his emphasis on transparency and integration with nature through the use of glass, laid a conceptual foundation for the development of modern transparent and composite structures. Although timber-glass composites were first explored in the late 1990s, Wright's ideas influenced the architectural direction that made such innovations possible.

Inspired by these concepts, this thesis explores how new materials and design approaches can support more sustainable and transparent structures. Timber-glass beams offer a potential solution for environmentally friendly building components such as ceilings, walls, or balconies where visual openness and structural function are both important.

The aim is to evaluate the possibilities and limitations of composite materials in beams, with a focus on achieving a balance between:

- Sustainability and sufficient load-bearing capacity,
- Environmental responsibility,
- Aesthetic quality within interior spaces.

In line with these architectural and structural goals, this thesis focuses on the resistance and stiffness of timber-glass composite beams. Their behavior

1. Introduction

was investigated through experimental testing and validated using numerical simulations in Abaqus. This dual approach was chosen to better understand how the beams respond under load, especially regarding displacement and load-displacement behavior.

1.2 Literature review

Composite timber–glass beams have been studied by several researchers in recent decades. Hamm [2] conducted one of the earlier systematic investigations into the structural performance of timber-glass composite elements. His work focused on the mechanical interaction between timber flanges and glass webs, including bending resistance and failure modes. Through physical testing and theoretical modeling, Hamm laid the groundwork for understanding how the two materials behave when bonded together under load, especially in terms of stiffness and crack development.

Kreher [3] and Natterer et al. [4] contributed significantly to the practical application of glass–timber composite technology. Their research included the design and construction of one of the first buildings to incorporate structural timber-glass beams, a hotel in Switzerland. This pioneering project demonstrated that such composite systems could be successfully implemented in real buildings, not only tested in laboratories. Their work also highlighted the importance of connection detailing, long-term durability, and stiffness performance under service loads.

Kozłowski et al. [5] studied the structural behavior of timber-glass composite beams through numerical analysis. Their research employed computational modeling to simulate cracks and brittle fractures in glass, using the finite element method to assess the effects of various parameters such as geometry, element size, and fracture energy on the overall performance of the structure. Based on these analyses, optimized models for wood-glass composite beams were identified. While the study primarily relied on numerical methods, the findings contribute valuable insights into the interaction between timber and glass, offering a foundation for further experimental validation and practical applications in structural engineering.

Blyberg and Serrano [6, 7] conducted several experimental and analytical studies to investigate the structural behavior of timber–glass composite beams. In their 2011 study [6], they performed four-point bending tests on fourteen timber–glass I-beams made of 10 mm fluted glass webs and laminated veneer lumber (LVL) flanges bonded with acrylate adhesive. The results showed that the composite system demonstrated good load-bearing capacity and ductility, with timber providing redundancy that helped prevent sudden failure after cracking of the glass. In a later study [7], Blyberg and Serrano presented analytical models and design approaches for such beams, emphasizing the importance of adhesive stiffness and partial composite action in predicting structural performance accurately.

1. Introduction

Similarly, Rajčić et al. [8] explored the influence of friction on the behavior and performance of prefabricated timber–glass composite systems, highlighting that friction between glass and wood significantly affects the system's structural behavior. These studies collectively support the effectiveness of timber-glass composite structures, emphasizing their ability to enhance structural integrity and failure resistance under various loading conditions.

Cruz et al. [9, 10, 11, 12] conducted several studies on the mechanical behavior and design of timber–glass composite beams. Their research focused on the safety and stability of these hybrid systems, with particular attention to laminated glass and adhesive connections. In one experimental study, twenty-three laboratory tests were performed on beams with different configurations to analyze their structural performance and failure behavior. The integration of a metal sheet or U-profile within the timber section was found to help redistribute tensile forces from the glass edge into the wooden part, increasing the overall strength and reducing stress concentrations. The results also showed that laminated glass maintains residual load-carrying capacity even after the first crack occurs, and that the heterogeneity of wood has only a limited effect on the overall strength of the composite beam. Among the tested adhesives, silicone was recommended due to its flexibility and ability to accommodate differential deformations between glass and timber, ensuring sufficient mechanical resistance. Overall, these studies demonstrated that the proposed timber–glass composite system can provide good stiffness, strength, and ductility, making it suitable for load-bearing architectural applications.

Premrov et al. [13] conducted an experimental evaluation of timber–glass composite I-beams under four-point bending. Their results showed that the inclusion of glass webs increased both the stiffness and strength of the beams compared to timber-only sections. It was observed that a glass beam with a height of only 240 mm could sustain considerable loads without premature failure.

Držečnik et al. [14] expanded this work by analyzing the influence of bonding boundary conditions on the load-bearing capacity and stiffness of timber–glass I-beams. Their studies demonstrated that the stiffness of the adhesive joint and cross-sectional configuration significantly affect the effective bending stiffness and post-cracking response. Furthermore, beams incorporating heat-strengthened and fully tempered glass were found to exhibit limited residual strength after fracture.

Rodacki and Furtak [15] carried out both experimental and numerical studies on the crack development and structural performance of timber–glass composite I-beams. In their research, the extended finite element method (XFEM) was employed to model glass cracking and adhesive behavior. The numerical results were validated through experimental tests, confirming that

1. Introduction

mesh density, glass fracture energy, and the adhesive model strongly influence simulation accuracy. Their additional 2018 experimental study focused on determining the load-bearing capacity and residual strength of composite beams under quasi-static and cyclic bending, showing that the adhesive layer plays a major role in redistributing stresses after cracking.

Buyuktaskin et al. [16] investigated the durability and long-term behavior of load-bearing timber–glass composite beams subjected to accelerated aging conditions. Their work highlighted that environmental exposure can significantly reduce bond strength and stiffness over time.

Unuk et al. [17] carried out experimental and numerical investigations on point connections in timber–glass composite structures. They introduced a novel system using aluminum inserts, epoxy adhesive, and self-tapping screws, which allowed for easy assembly and disassembly of the glass element. Their tests showed promising shear load capacity and slip behavior, although connection failure occurred primarily in the fasteners rather than the glass. This work highlights the importance of connection detailing for the performance and safety of timber–glass composites.

Gemi et al. [18] explored the behavior of pultruded glass-fiber-reinforced polymer (GFRP) composite beams filled with hybrid fiber-reinforced concrete. Although their work did not directly involve timber–glass composites, the methodology and analytical modeling provide useful insights for evaluating hybrid structural systems under four-point bending.

1.3 Aim and purpose

In the thesis, an experimental test series is performed on glass-timber composite beams. Laminated glass is used for the web with different combinations of float and hardened glass. The tests are then compared to results from finite element simulations.

Using laminated glass is a novelty in this field. The thesis therefore helps to know more about this type of beams and helps to introduce timber-glass composites as structural elements.

1.4 Hypothesis and limitations

Previous research on timber–glass composite beams has mostly focused on beams with a single glass web. In this study, however, laminated glass webs are used. The hypothesis is that laminated webs offer improved safety due to built-in redundancy within the system, potentially allowing the structure to maintain integrity even after partial glass failure.

1. Introduction

The main limitation of this research is the limited number of tested samples. Additionally, only three different types of lamination combinations were studied, using one specific cross-sectional geometry, one adhesive type, and one type of flange material. These constraints limit the generalizability of the findings but still provide valuable insight into the structural behavior of laminated timber–glass beams.

2. Material and Methods

In this section, the material properties of the constituents will be described: glass for the web, timber for the flanges, as well as the adhesive that combines both. In the end, the method how to calculate bending stiffness from the experiments is explained.

In this study, a combination of timber and glass was selected for use in structural beams. Specifically, three different configurations were used to form composite timber–glass beams: double-layer float glass, double-layer heat-strengthened glass, and a combination of one layer of float glass and one layer of heat-strengthened glass. A laboratory experiment was designed to examine their deflection and bending stiffness, allowing for evaluation of both the advantages and limitations of these materials.

Beyond their architectural aesthetics, timber and glass have demonstrated favorable structural properties, particularly in terms of deflection behavior and load-bearing capacity. The glass types used either individually or in combination are float glass and heat-strengthened glass, both laminated using PVB film.

The flange material is laminated veneer lumber (LVL), which is bonded to the glass web using adhesive. The connection between the timber flanges and the glass web is achieved with a 2 mm layer of Silicone S500 adhesive, as shown in Figure 2.

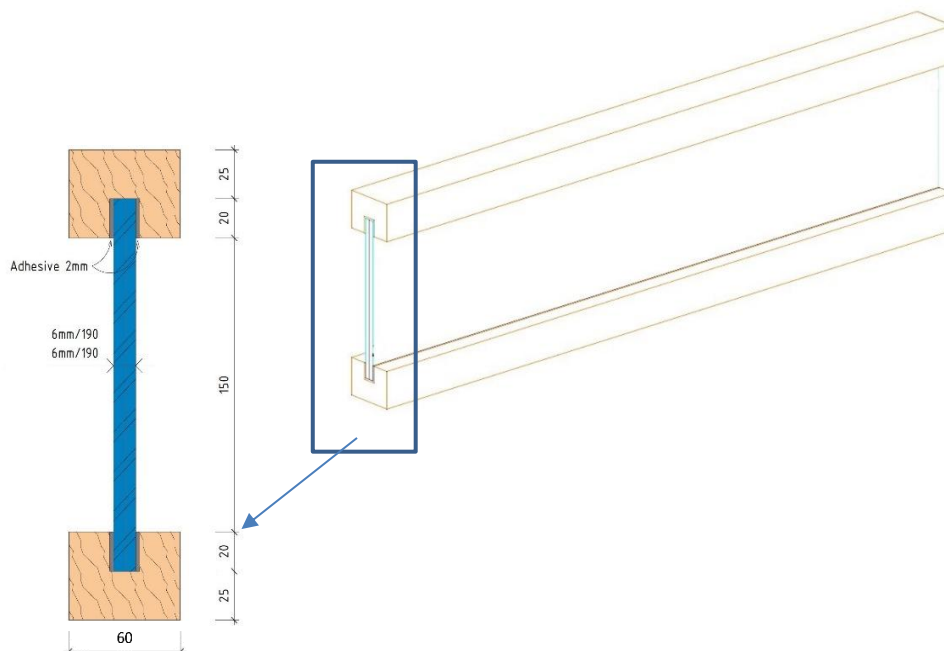


Figure 2: Cross section of composite glass-timber beam.

2. Material and Methods

2.1 Material properties

2.1.1 Glass

Glass was traditionally used only for windows and partitions, but today, with advances in technology and the demand for innovative materials, it is increasingly applied in new structural systems, such as timber–glass composites and translucent concrete.

Glass has the same stiffness in tension and compression, since its Young's modulus is constant and isotropic. However, its strength behavior differs in tension and compression. Glass is more sensitive in tension, where small surface flaws can grow into cracks and cause sudden brittle failure without prior deformation or warning. Because of this, using glass as a structural material requires special safety considerations.

To improve performance and safety, different types of engineered glass have been developed. Heat-strengthened glass, for example, provides greater load-bearing capacity and better resistance to thermal and mechanical stresses compared to ordinary float glass. Other widely used types include tempered glass, laminated glass, and safety glass. Tempered glass is strengthened through thermal treatment, and when it breaks, it shatters into small, blunt fragments instead of sharp shards. Laminated glass is formed by bonding two or more layers of glass with an interlayer such as polyvinyl butyral (PVB). Even after breakage, the fragments adhere to the interlayer, reducing the risk of injury and preserving residual strength.

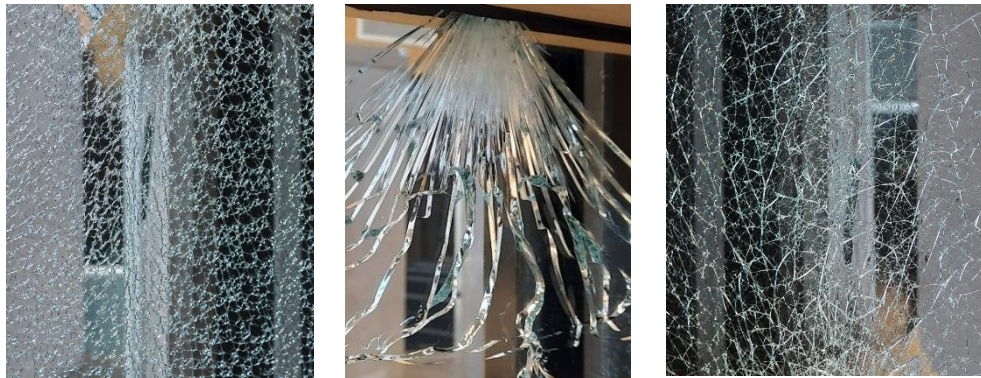
In modern construction, glass is used not only in façades, windows, and interior walls but also in selected load-bearing applications. Float glass, heat-strengthened glass, and laminated glass are the most common types, each selected according to structural and safety requirements.

Float glass is produced by pouring molten glass onto a bath of molten tin, which allows it to spread into a flat, uniform sheet. This results in a smooth surface and high optical clarity, making it ideal for glazing applications. However, because float glass lacks internal stresses, it is relatively fragile and prone to breakage under impact or thermal shock.

Tempered glass is manufactured by heating float glass to approximately 600–700 °C and then rapidly cooling it with high-pressure air jets. This process, known as thermal tempering, induces compressive stresses on the outer surfaces while the core remains in tension. These internal stresses increase strength by a factor of four to five compared to ordinary float glass, making it resistant to impact, bending, and thermal stress. When broken, it fragments into small blunt-edged pieces, reducing the risk of injury. Due to these properties, tempered glass is commonly used in windows, doors, shower enclosures, and automotive glazing. However, it cannot be cut or drilled after tempering, as it will shatter immediately.

2. Material and Methods

Laminated glass is produced by bonding two or more layers of glass with an interlayer, typically polyvinyl butyral (PVB) or ethylene-vinyl acetate (EVA). The assembly is fused under heat and pressure in an autoclave, creating a durable, impact-resistant product. Laminated glass provides excellent safety because the interlayer holds the fragments together after breakage, preventing shattering. It also offers sound insulation, UV protection, and resistance to forced entry, making it suitable for skylights, car windshields, and structural glazing. While laminated glass offers superior safety and durability, it is generally heavier and more costly than other glass types due to its layered construction (see Figure 3).



Tempered glass

- Shatter to entire sheet due to internal stress or a strong impact on edges
- Producing long sharp splinters

Annealed glass

- Crushed completely under higher level of impact force
- Few pieces remain in the frame

Laminated glass

- Possible to crack under pressure
- Remain in place
- Stick to PVB layer

Figure 3: Examples of three types of glass.

Glass is an amorphous and isotropic material, meaning its mechanical properties are the same in all directions. Unlike crystalline materials, it does not have a regular atomic structure. Its key mechanical properties include Young's modulus, which reflects stiffness in both tension and compression, and the shear modulus, which characterizes its resistance to shear deformation. According to Hamm (2000) [2] and Cruz & Pequeno (2008) [9], glass has very high compressive strength, typically around 300 MPa, but it is brittle and comparatively weak in tension. This weakness is caused by microscopic surface flaws that can propagate into cracks and lead to sudden brittle fracture. The tensile strength of glass is usually in the range of 20–90 MPa, although theoretically it could be much higher if flaws were absent. While glass can deform elastically under small loads, it lacks plastic behavior and therefore fails abruptly once its strength limit is reached. A summary of the main mechanical properties of float and heat-strengthened glass used in this study is provided in Table 1.

2. Material and Methods

Table 1: Mechanical properties of annealed float glass and heat-strengthened glass (adapted from Hamm [2] and Cruz & Pequeno [9]).

	Float glass (Annealed)	Heat-strength glass	Unit
Density	2500	2500	kg/m ³
Young's modulus	70	70	GPa
Poisson's ratio	0.18	0.23	
Shear modulus	30	28	GPa
Tensile strength	20	50	MPa

2.1.2 PVB film

Laminated glass consists of at least two layers of heat-strengthened or float glass with an interlayer material in between. In this study, polyvinyl butyral (PVB) was used as the interlayer. Other interlayer materials, such as ethylene-vinyl acetate (EVA) and ionoplast films, are also common, but these were not considered in this research. PVB films are typically manufactured in thicknesses of 0.38 mm, 0.76 mm, or 1.52 mm.

The interlayer plays a critical role in safety by keeping the glass intact after breakage, as fragments adhere to the film rather than scattering. Compared to monolithic glass, laminated glass provides significantly higher impact resistance. In addition, the PVB layer reduces sound transmission and blocks a considerable portion of harmful UV radiation (Hamm [2]; Ebnesajjad [19]).

Because of these properties, laminated glass is widely used in applications requiring both safety and durability, such as high-rise buildings, glass floors, windshields, and other structural glazing systems. The mechanical properties of PVB are strongly influenced by temperature and loading due to its viscoelastic nature.

Table 2: Mechanical properties of PVB film (adapted from [21, 22]).

	PVB	Unit
Density	950	kg/m ³
Young's Modulus	2	MPa
Poisson's Ration	0.4	
Failure stress	28	MPa
Typical short-term tensile yield strength	20	MPa
Typical long-term tensile yield strength	3–5	MPa

2. Material and Methods

2.1.3 Wood

Wood is a natural, sustainable material that offers many advantages in construction. It is renewable, durable, and aesthetically pleasing, making it a widely preferred material compared to conventional alternatives. In addition to being cost-effective, wood has high structural strength and excellent load-bearing capacity, which makes it suitable for a variety of engineering applications. Structurally, timber is an orthotropic material, meaning its mechanical properties vary along three principal directions due to its fiber orientation. This results in anisotropic behavior under different loading conditions. Its ductility in compression further enhances its performance, making it highly effective in load-bearing applications.

Given these properties, wood plays a crucial role in composite systems by providing load-bearing capacity and structural stability. In timber-glass composite beams, timber is typically used as the flange element, where it effectively resists compressive stresses and contributes to overall stiffness. The use of grooves and adhesive bonding enables efficient load transfer between components, enhancing the structural performance of the system. In addition, the ductility of timber improves the overall robustness of the beam, allowing it to maintain stability under loading.

The timber used in this study is laminated veneer lumber (LVL), an engineered wood product known for its strength, uniformity, and reliability in structural applications. LVL is manufactured by bonding multiple layers of thin softwood veneers (typically about 3 mm thick) with phenol-formaldehyde adhesive under heat and pressure. This controlled process produces a highly stable and uniform material that resists warping and delivers consistent mechanical performance.

The production process of veneer consists of four stages.

- Veneer Production: Logs are rotary peeled to produce veneer sheets, typically 3.2 mm thick for LVL production.
- Drying and Grading: Veneer sheets are dried to the required moisture content and graded for quality.
- Adhesive Application and Assembly: Adhesive is applied, and veneers are stacked with grains oriented in the same direction to enhance strength.
- Pressing and Curing: The stack is pressed under heat and pressure, curing the adhesive and forming a solid LVL billet [20] [21].

The LVL used in this study corresponds to Kerto-S, where all veneer layers are aligned parallel to the grain direction to maximize stiffness and strength

2. Material and Methods

along the beam's length. The characteristic and mechanical properties are presented in Table 3 [25].

Table 3: Characteristic and mechanical properties of Kerto-S LVL (adapted from [25]).

Properties	Symbol	Value	Unit
Characteristic density	ρ_k	480	kg/m ³
Mean density	ρ_{mean}	510	kg/m ³
Modulus of elasticity (parallel to grain)	$E_{0,\text{mean}}$	13 800	MPa
Modulus of elasticity (perpendicular to grain)	$E_{90,\text{edge,mean}}$	430	MPa
Shear modulus	$G_{0,\text{mean}}$	600	MPa
Tensile strength (parallel to grain)	$f_{t,0,k}$	35	MPa
Tensile strength (perpendicular to grain)	$f_{t,90,\text{edge,k}}$	0.8	MPa
Compression strength (parallel to grain)	$f_{c,0,k}$	35	MPa
Compression strength (perpendicular to grain)	$f_{c,90,\text{edge,k}}$	6	MPa
Shear strength	$f_{v,90,\text{edge,k}}$	4.1	MPa

2.1.4 Adhesive

Adhesives are non-metallic chemical materials that allow objects and surfaces to bond permanently. They can be derived from natural sources or synthesized through industrial processes, and depending on their chemical structure and properties, they are applied in different areas of construction.

Silicone is one of the most commonly used adhesives in construction due to its chemical versatility and performance. It is composed of polymers formed during curing reactions such as step-growth or chain-growth polymerization. Its unique chemical structure, based on a siloxane backbone (Si–O–Si) with organic side groups, makes it a hybrid between organic and inorganic materials. This structure provides low surface energy, which improves wetting and adhesion, and high flexibility, which allows it to absorb stress. Together, these features enable silicone adhesives to achieve strong bonding and reliable performance under dynamic loads [19, 22, 26].

Adhesives are typically classified into one-component and two-component types. One-component adhesives, such as silicone and polyurethane, cure when exposed to air, moisture, or heat without requiring mixing. In contrast, two-component adhesives, such as acrylates, require mixing before application to initiate curing.

2. Material and Methods

Bending strength is a key parameter in evaluating the structural performance of timber–glass composite beams, as it defines their ability to resist deformation under load. In these systems, adhesives such as silicone play an important role in transferring stresses between materials. Although the bending strength of silicone is relatively low compared to structural materials, usually in the range of 2–5 MPa depending on the formulation, its flexibility, adhesion capacity, and ability to maintain bond integrity under load make it suitable for composite applications [19, 22, 26].

Previous researchers such as Hamm [2] and Cruz & Pequeno [9] have investigated the use of different adhesives in timber–glass beams. Based on these studies and the requirements of this research, a silicone adhesive was selected. In this study, SikaSil SG-500 was used.

Main purposes of using silicone adhesive:

- Flexibility combined with sufficient strength and adhesion
- Resistance to various weather conditions
- Uniform distribution of forces at the interface

The mechanical and physical properties of the SG-500 silicone adhesive used in this study are presented in Table 4. These values, which include density, tensile strength, and modulus of elasticity, provide the necessary input parameters for both experimental interpretation and numerical modeling of the composite beams.

Table 4: Characteristic properties of SikaSil SG500 (adapted from [29] and manufacturer’s technical data sheet).

	Density mixed	Tensile strength	Modulus of elasticity
unit	kg/l	MPa	MPa
Silicon SG500	1.37	2.2	3.17

2.2 Calculation of beam bending stiffness

Structures exhibit different types of stiffness, including axial, torsional, shear, and bending stiffness. These characteristics depend on the mechanical properties of the materials. Among the most important are the Young’s modulus E , which governs axial and bending stiffness, and the shear modulus G , which governs shear and torsional stiffness. In particular, the modulus of elasticity E plays a key role in determining overall structural stiffness, as it reflects the material’s ability to resist deformation under load.

2. Material and Methods

In this experiment, the applied load is vertical and symmetric, so torsional effects can be neglected. Similarly, axial stiffness is not considered since the beam primarily undergoes vertical deflection rather than axial deformation.

Shear stiffness, however, is significant in composite timber–glass beams. Because the system combines materials with different mechanical properties, shear deformations influence the strain distribution and load-bearing capacity. This effect becomes more pronounced when the stiffness contrast between timber and glass is large.

Despite this, the main focus in this study is on bending stiffness. Bending stiffness describes the beam’s resistance to deflection under bending moments and is expressed as the product of the material’s elastic modulus and the second moment of area (EI). It can be evaluated by measuring vertical deflection under known loads [23].

The bending stiffness of the composite beams was evaluated using a four-point bending test, which clearly distinguishes between bending and shear effects. In this setup, two equal loads are applied symmetrically at equal distances from the supports, creating a constant moment region between the loading points. This configuration minimizes shear deformation in the central span, allowing more accurate evaluation of bending stiffness.

Both global and local displacements were measured. Global displacement refers to the overall deflection of the beam at points such as the midspan or directly under the load. Local displacement was measured at closer intervals using displacement sensors along the beam, capturing detailed strain and deflection behavior in the composite region. These measurements enabled the back-calculation of effective bending stiffness, providing insight into the structural performance of the timber–glass system. Figure 4 shows the test beam setup.

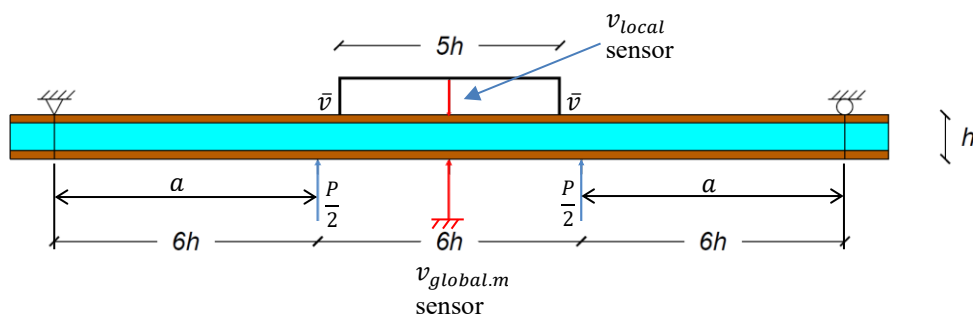


Figure 4: Measurement and loading position of composite beam.

2. Material and Methods

To calculate the local displacement at a specific point along the beam under four-point bending, the total displacement is divided into two parts:

$$v_{01} = \frac{P \times L \times b}{6EI} \left(\left(1 - \frac{b^2}{L^2} \right) x - \frac{x^2}{L^2} \right) \quad (2.1)$$

$$v_{12} = \frac{P \times a}{6EI} \left(-a^2 + \left(2L + \frac{a^2}{L} \right) x - 3x^2 + \frac{x^3}{L} \right) \quad (2.2)$$

where:

v_{01} : displacement measured between support and load point.

v_{12} : displacement measured at the center of the beam between two loads.

P : total load.

a : distance from the support to the load point ($a = 6h$).

L : span length ($L = 18h$).

h : beam height.

b : distance from the support to the first load point.

x : position along the beam measured from the left support.

E : Young's modulus,

I : second moment of inertia.

The total local displacement \bar{v} is then the sum of these two contributions:

$$\bar{v} = v_{01} + v_{12} \quad (2.3)$$

Global displacement at the middle of the beam is calculated as:

$$v_{global.m} = \frac{P \times a}{24EI} (3L^2 - 4a^2) \rightarrow x = \frac{L}{2} \quad (2.4)$$

2. Material and Methods

Global displacement at the load point is calculated by using equation below:

$$v_{global.load.p} = \frac{P \times x}{6EI} (3aL - 3a^2 - x^2) \quad \rightarrow 0 > x > a \quad (2.5)$$

Local displacement at the middle of the beam is calculated by subtracting $v_{global.m}$ and \bar{v} :

$$v_{local} = v_{global.m} - \bar{v} \quad (2.6)$$

Displacement under a point load in four-point bending at the load point is:

$$v_{load.p} = \frac{P \times a^2(3L - 4a)}{6EI} \quad (2.7)$$

$v_{load.p}$ is the vertical displacement measured directly under one of the load application points

The bending stiffness, EI , represents the resistance of the beam to bending. It affects how much the beam deflects under an applied load and is related to the slope of the load–displacement curve. In composite beams, bending stiffness is treated as a combined property rather than separating the elastic modulus E and the moment of inertia I , since the materials have different mechanical properties. Using displacement measurements taken at different positions along the beam, the effective bending stiffness EI was calculated from the experimental results, as summarized in Table 5.

Table 5: Calculation of bending stiffness (EI) based on load-point, local, and global displacement measurements in four-point bending.

Calculation based on displacement	Load point	Local	Global
Bending stiffness EI	$\frac{90Ph^3}{v_{load.p}}$	$\frac{75Ph^3}{8v_{local}}$	$\frac{207Ph^3}{2v_{global.m}}$

3. Experimental testing

The evaluation of the beams in this project was conducted through laboratory testing and computer simulations. The results from both methods were subsequently analyzed and compared. The experimental procedure focused on examining and calculating the load-bearing stiffness of the beams under load, as well as selecting appropriate materials to support the investigation. The load–displacement relationship was calculated and illustrated in a diagram. The stiffness of the beams was studied based on this diagram and compared with the simulated software results. The study includes the determination of the failure stress and modulus of elasticity of glass tested in a vertical position at various times. For heat-strengthened glass, residual stress levels were also evaluated.

3.1 Test set-up

In this research, an experimental investigation was carried out using composite timber–glass beams. The materials used in the test setup include:

- Float Glass: Density of 2500 kg/m^3 , Young's modulus of 70 GPa, Poisson's ratio of 0.18, shear modulus of 29.66 GPa, and typical tensile strength of 45 MPa.
- Heat-Strengthened Glass: Density of 2500 kg/m^3 , Young's modulus of 70 GPa, Poisson's ratio of 0.23, shear modulus of 28.46 GPa, and yield stress of 50 MPa.
- PVB film with density of 950 kg/m^3 , Young's modulus of 3.17 MPa, Poisson's ratio of 0.4, and tensile yield strength of 3-5 MPa.
- Thin wood based on LVL (Laminated Veneer Lumber) with a density of 510 kg/m^3 and a modulus of elasticity of 13.8 GPa.
- SikaSil SG500 adhesive with a density of 1370 kg/m^3 , tensile strength of 2.2 MPa, and modulus of elasticity of 3.17 MPa.

The experimental setup consisted of a four-point bending configuration using a hydraulic test machine. Each beam was simply supported at both ends, with two equal point loads applied symmetrically to simulate uniform bending in the central span. This setup allowed accurate measurement of deflection and bending stiffness under controlled loading conditions. Displacement sensors and force transducers were used to monitor structural response throughout the test, the test setup is shown in Figure 5.

3. Experimental testing

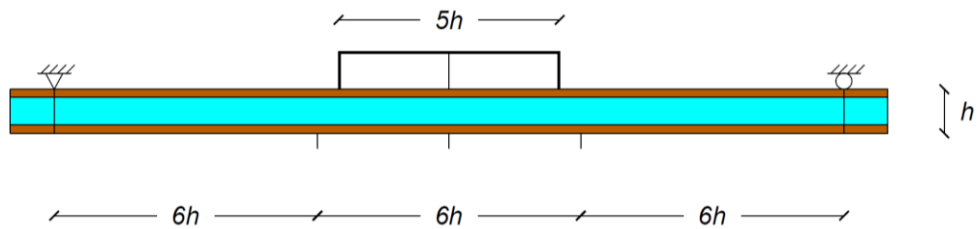


Figure 5: Four-point bending test setup of the timber–glass composite beam, including the loading system and displacement sensors.

A total of nine I-shaped timber–glass composite beams were tested in this study. All beams had the same geometric configuration, with identical dimensions and material properties for the timber flanges and the adhesive layer. The only variable among the three groups was the type of glass used in the web. Each beam consisted of two 6 mm glass panes laminated together.

- Beams 1–3 contained double float glass (6 mm + 6 mm).
- Beams 4–6 used a combination of one float glass and one heat-strengthened glass.
- Beams 7–9 contained double heat-strengthened glass (6 mm + 6 mm).

The group of test specimens is displayed in Figure 6.

3. Experimental testing



Figure 6: The nine tested composite timber-glass I-shaped beam specimens.

Each beam featured two timber flanges made of LVL with a rectangular cross-section of 60 mm (width) \times 45 mm (height). A central groove with dimensions of 17 mm \times 20 mm was cut into each flange to hold the glass web. The beam's detailed geometry is illustrated in Figure 7, and all geometric values are summarized in Table 6.

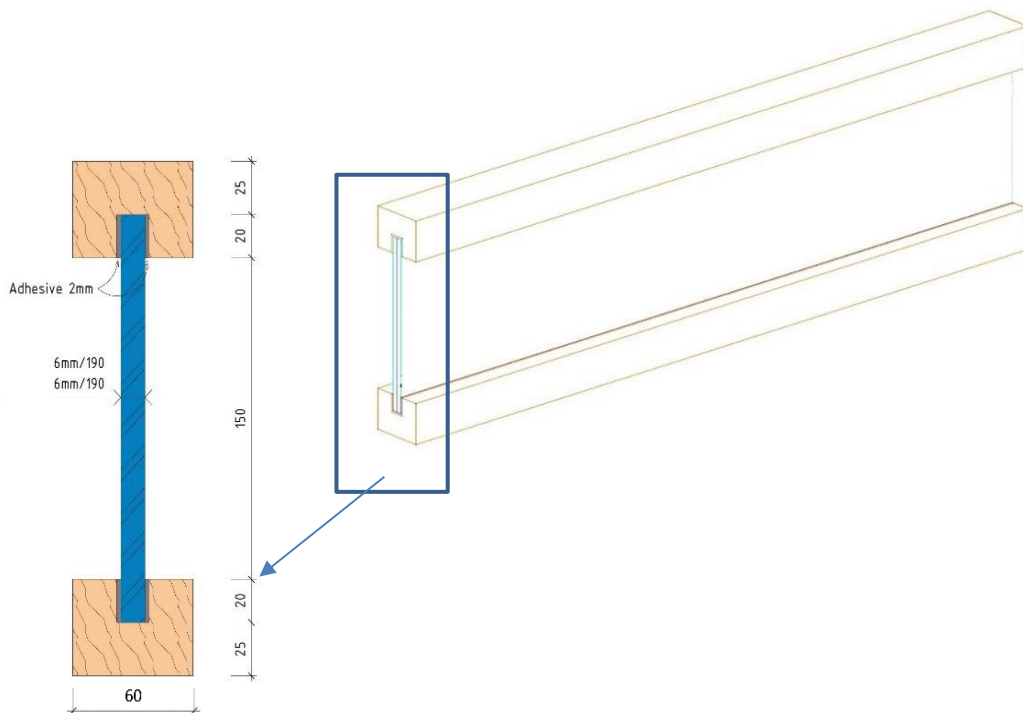


Figure 7: Cross-section and dimension of the timber-glass I-shaped beam.

3. Experimental testing

Table 6: Geometry of glass-timber composite beams.

Type	length (mm)	height (mm)	Flange (mm)		Glass thickness (mm)	Glass type
			height	width		
1	4800	240	45	60	6+6	Float + Float
2	4800	240	45	60	6+6	Float + Heat-strengthened
3	4800	240	45	60	6+6	Heat-strengthened + Heat-strengthened

Four strain gauge sensors were installed at the midspan of the beams, positioned on both sides of the web and the flanges for Group 1 beams with double float glass, and on the float glass side for beams with one float glass layer combined with one heat-strengthened glass layer (see Figure 8). By placing the gauges on both the glass web and the timber flanges, the strain distribution in both the compression and tension zones of the cross-section could be measured. In addition, this setup allowed the determination of the maximum strain and tensile stress in the glass web at the point of failure.

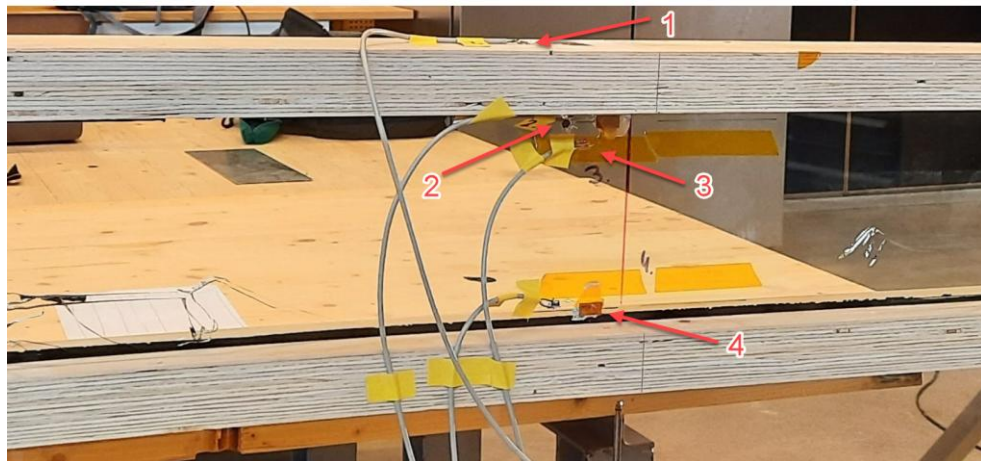


Figure 8: Strain gauge locations at the midspan of the timber–glass composite beam: (1) top of the upper timber flange – flange tension zone, (2) below the upper flange – flange compression zone, (3) upper side of the glass web – glass tension zone, and (4) lower side of the glass web – glass compression zone.

Four-point bending tests were performed using a universal testing machine. Before installation, the beam height was carefully re-measured at the supports, loading points, and displacement sensor positions. In addition, the glass thickness of each sample was measured to ensure accuracy. The beams were mounted on the test device using two simple supports, allowing movement only in one direction. The loading points were positioned at a distance of $6h$ from each end of the beam. Figure 9 illustrates the four-point bending test setup.

3. Experimental testing



Figure 9: Load test machine used for four-point bending tests. The yellow arrows indicate the locations of the two symmetrically applied point loads on the beam.

In addition to the four strain gauges, two displacement sensors were installed during the experiment. One sensor was positioned at the top center of the beam to measure local displacement (Figure 10), while the other was placed beneath the beam to record global displacement (Figure 11). Both local and global displacements were continuously recorded at multiple time steps throughout the loading process. Local displacement was measured only until the first visible crack appeared. Within this range, the beam response was considered linear, allowing the initial elastic bending stiffness to be calculated from the measured local displacement.

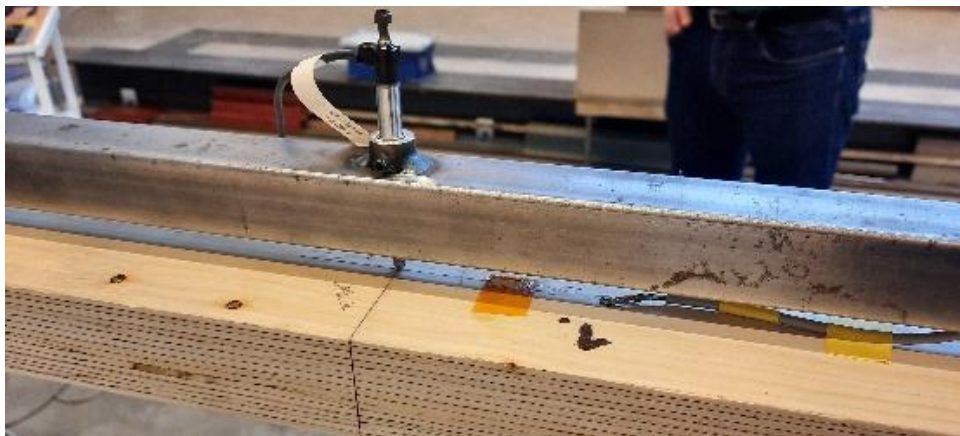


Figure 10: Setup of displacement sensor for local displacement measurement (top of beam).

3. Experimental testing



Figure 11: Setup of displacement sensor for global displacement measurement (bottom of beam).

Each beam was carefully cleaned to remove any adhesive residue or surface contamination from the glass. All specimens were installed under identical conditions to ensure consistency and comparability of results. Ambient temperature and humidity were neither controlled nor recorded during the experiments and are therefore not considered in the analysis.

The tests were successfully completed, and the obtained results met the expectations for determining the relevant parameters. The predictable behavior of the specimens, together with the clear outputs from both the testing machine and the software, provided reliable data for accurate calculations.

3.1.1 Beam group 1 (float-float)

Beams constructed with double float-glass exhibited linear load–displacement behavior up to the initiation of the first crack in the glass web. After cracking, the response transitioned into a nonlinear phase, as evident in the experimental graphs. This indicates that the beams provided a form of warning mechanism prior to failure. Cracks initiated progressively in the tension zone under increasing load, giving visible signs of impending failure rather than collapsing suddenly.

The first cracks typically appeared symmetrically at the load application points, which were spaced 1440 mm apart. Additional cracks subsequently formed approximately 300 mm from the midspan, as shown in Figure 12. Despite the presence of multiple cracks, the beams continued to carry load and retained their structural capacity until final failure. Figure 13 shows the overall condition of the beam after failure.

3. Experimental testing



Figure 12: Crack development in the glass web near the load application points, located in the shear-dominated region between the supports and the point loads.



Figure 13: Overall view of the beam after failure showing the final crack distribution and the beam configuration at failure.

The diagram based on local displacement (Figure 15) shows significantly lower maximum load values compared to the global displacement diagram (Figure 14). This difference arises because the local displacement was measured using a sensor positioned directly between the glass web and timber flange, capturing only a small section of the beam and reflecting the initial elastic deformation phase. Once the adhesive or glass began to fail, the local sensor lost proper contact, and further measurements were no longer possible.

Consequently, the local displacement data ends prematurely, before the beam reached its full load-carrying capacity or failure. By contrast, the global displacement, recorded from the testing machine's crosshead, continued until final failure and represents the overall deformation response of the entire beam system.

3. Experimental testing

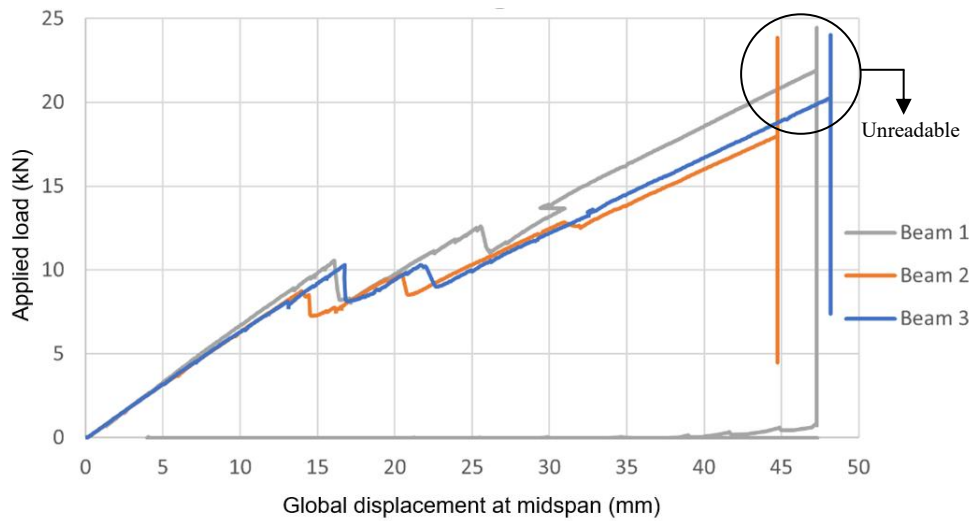


Figure 14: Applied load–global displacement curves for double-layer float glass beams, where the global displacement represents the midspan displacement of the beam.

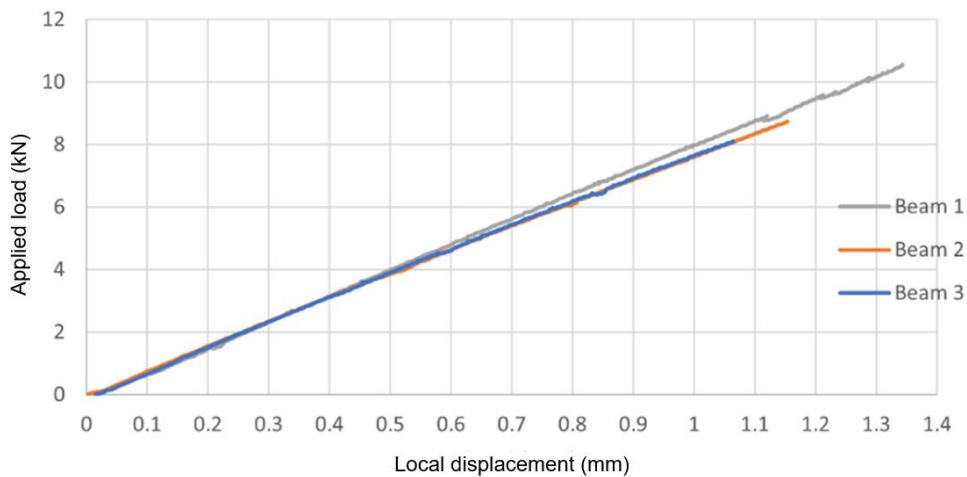


Figure 15: Applied load–local displacement curves for double-layer float glass beams, where the local displacement represents the displacement measured between the support and the load point.

Global displacement for these beams at the first crack was 13.47, 14.43, and 13.12 mm with the total force of 8.92, 8.50, 7.90 kN for beams group one (experiments number 1-3). The maximum total force before failure was 21.94, 23.87, and 24.00 kN on specimen numbers 1-3. The results of the beams with double float-glass are presented in Table 7.

3. Experimental testing

Table 7: Results of the beams with double float-glass.

Specimen (Sample number)	Total force at first crack (kN)	Global displacement at first crack (mm)	Maximum total force before failure (kN)	Maximum global displacement at failure point (mm)
1-1 (1)	8.92	13.47	21.94	> 47 mm
1-2 (2)	8.50	14.43	23.87	> 44 mm
1-3 (3)	7.90	13.12	24.00	> 48 mm
Mean value	8.44	13.67	23.27	> 45 mm

3.1.2 Beam group 2 (heat-strengthened -float)

Beams in this group were composed of one layer of float glass and one layer of heat-strengthened glass. The results indicate that this configuration exhibited a higher load capacity compared to beams with double float glass. Cracks developed exclusively on the float glass side, while the heat-strengthened glass layer remained intact at least until final failure.

The location of the first cracks in the float glass was predictable: similar to the behavior of the beams in Group 1, they appeared initially at the loading points and subsequently at approximately 300 mm from the midspan. Despite these cracks, the beams were able to maintain their load capacity through the contribution of the heat-strengthened glass layer until ultimate collapse.

The crack positions observed during testing are shown in Figure 16 and Figure 17, while Figure 18 shows the beams remaining upright after failure, highlighting the stabilizing role of the timber flanges in preserving the structural integrity of the beam after glass cracking.



Figure 16: Crack formation in the tested beam.

3. Experimental testing



Figure 17: Crack formation in the tested beam showing different perspectives of the same specimen.

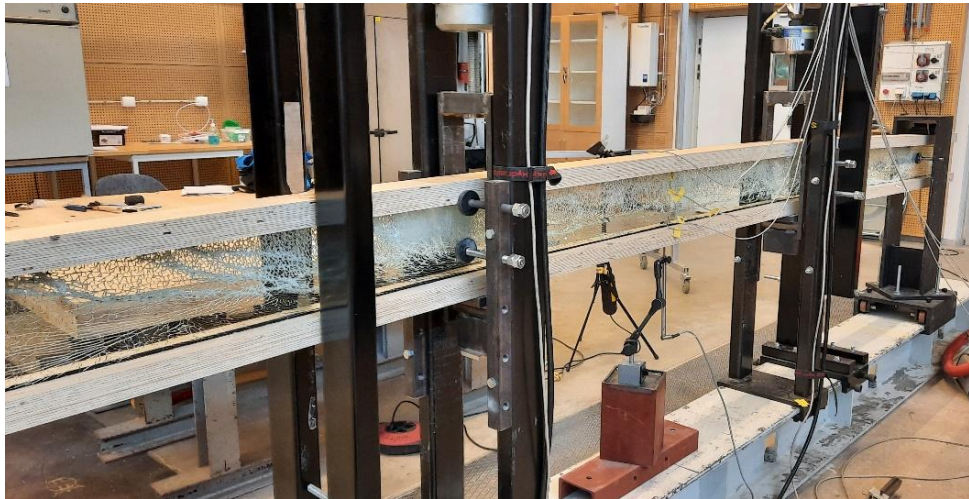


Figure 18: Beams standing after failure of the beams with one-layer float glass and one-layer heat-strength glass.

For specimens 4–6, the maximum total forces were 26.52 kN and 24.46 kN, corresponding to maximum global displacements of 46.87 mm and 43.26 mm, respectively, at final collapse. In specimen 5 (Beam 2 in Group 2), the maximum global displacement could not be recorded, as loading was stopped before complete failure. This behavior is illustrated in Figure 19.

At the onset of the first visible crack, the global displacements were 15.73 mm, 15.11 mm, and 15.29 mm, corresponding to total forces of 9.87 kN, 9.43 kN, and 9.66 kN for specimens 4–6, respectively. The load–local displacement relationship is presented in Figure 20, showing the initial elastic response prior to failure.

3. Experimental testing

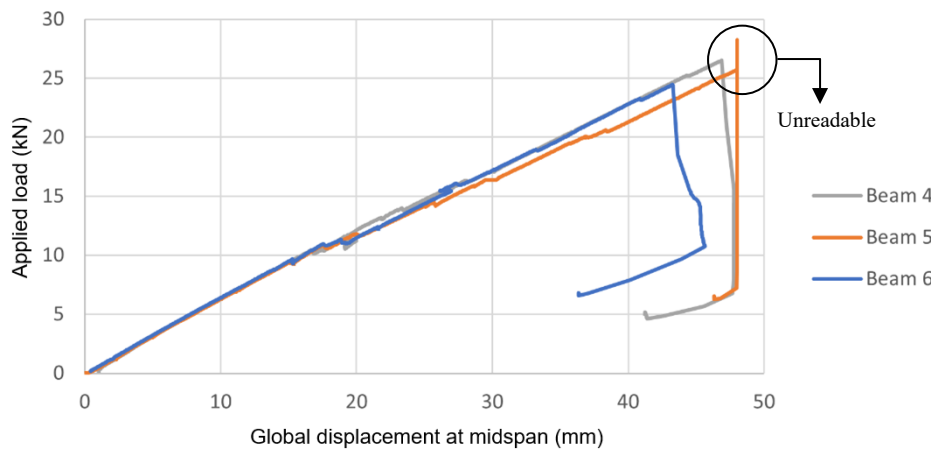


Figure 19: Applied load–global displacement curves for beams with one-layer float glass and one-layer heat-strengthened glass, where the global displacement represents the midspan displacement of the beam.

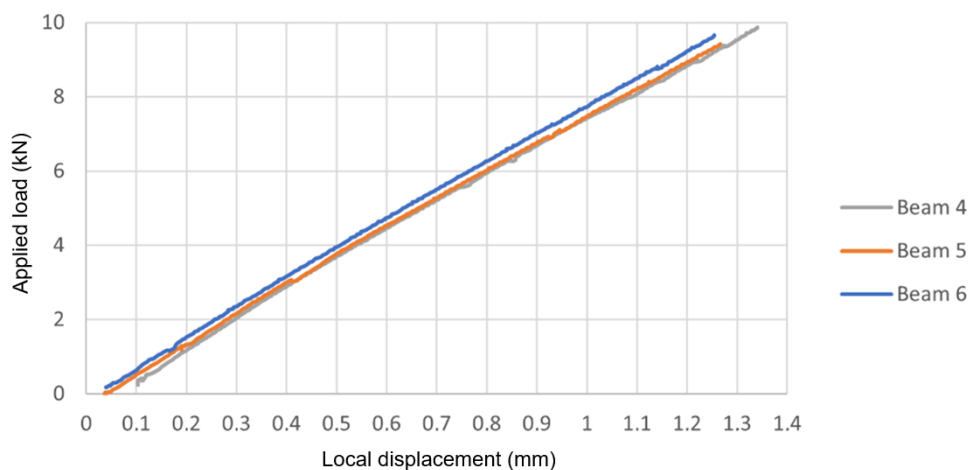


Figure 20: Applied load–local displacement curves for beams with one-layer float glass and one-layer heat-strengthened glass, where the local displacement represents the displacement measured between the support and the load point.

As shown in the graph in Figures 18 and 19, the heat-strengthened glass continued to carry load and maintain the stability of the beams even after cracks had developed in the float glass. Table 8 summarizes the test results for the beams with one layer of float glass combined with one layer of heat-strengthened glass.

3. Experimental testing

Table 8: Results of the beam with one-layer float and one-layer heat-strength glass.

Specimen (Sample number)	Total force at first crack (kN)	Global displacement at first crack (mm)	Maximum total force before failure (kN)	Maximum global displacement at failure point (mm)
2-1 (4)	9.87	15.73	26.52	> 46 mm
2-2 (5)	9.43	15.11	28.26	> 48 mm
2-3 (6)	9.66	15.29	24.46	> 43 mm
Mean value	9.65	46.13	26.41	> 45 mm

3.1.3 Beam group 3 (strengthened-strengthened)

The beams constructed with double layers of heat-strengthened glass exhibited a linear load–displacement relationship up to the point of sudden failure. In contrast to the beams with double float glass (Group 1), no visible cracks appeared prior to collapse. These specimens carried load steadily until reaching their maximum capacity, after which they failed abruptly in a brittle manner without warning. Figures 21 and 22 show the crack patterns and the post-failure condition of the beams.



Figure 21: Crack patterns of beams with double-layer heat-strengthened glass.

3. Experimental testing



Figure 22: Beams standing after failure of double-layer heat-strengthened glass beams.

The results indicate that beams in this group exhibited a much higher load capacity compared to the other two groups. Specimens 7–9 showed greater resistance due to the use of heat-strengthened glass. The maximum total forces recorded were 36.05 kN, 32.77 kN, and 34.69 kN, which ultimately caused fracture of the glass and led to final collapse. Figures 23 and 24 present the load–displacement curves for global and local measurements, respectively.

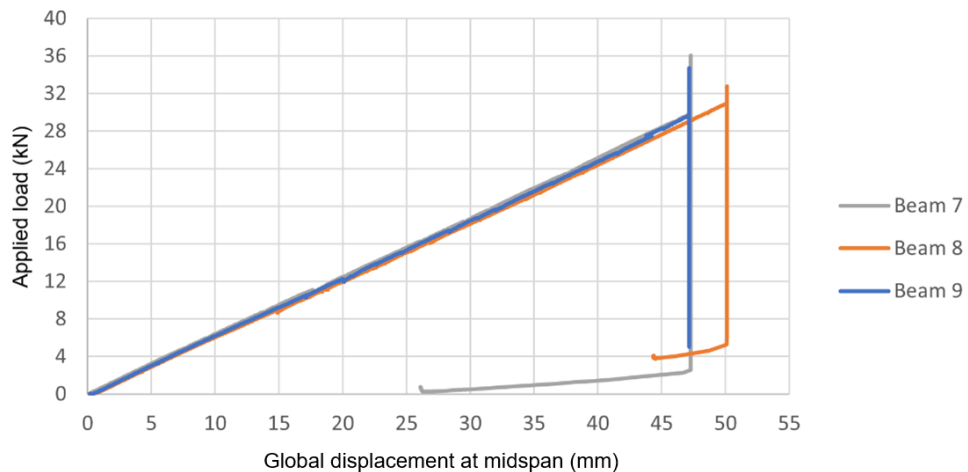


Figure 23: Applied load–global displacement curves for double-layer heat-strengthened glass beams, where the global displacement represents the midspan displacement of the beam.

3. Experimental testing

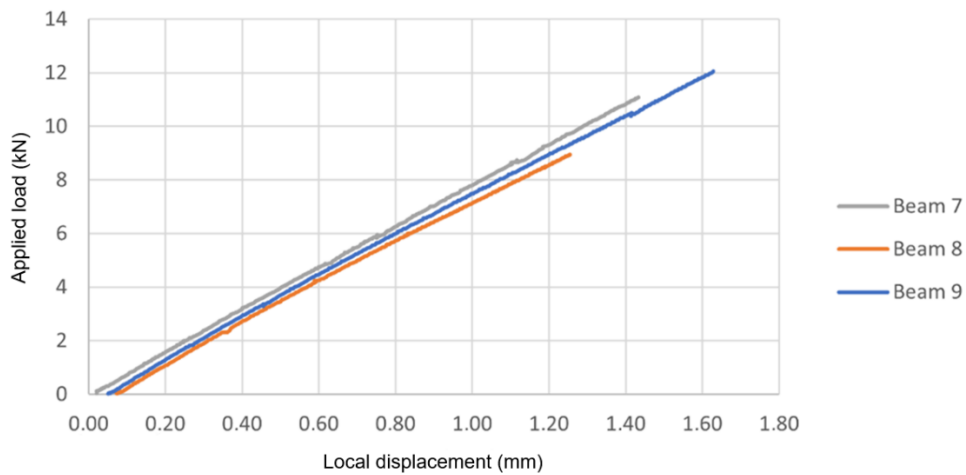


Figure 24: Applied load–local displacement curves for double-layer heat-strengthened glass beams, where the local displacement represents the displacement measured between the support and the load point.

As shown in Figure 24, the local displacement was recorded only within the first 1–2 seconds of loading. In this group, the maximum load capacity was significantly higher than in the other beam groups. The detailed results for the beams with double heat-strengthened glass are presented in Table 9.

Table 9: Results of the beam with double heat-strength glass.

Specimen (Sample number)	Maximum total force before failure (kN)	Maximum global displacement at failure point (mm)
3-1 (7)	36.05	> 47 mm
3-2 (8)	32.77	> 50 mm
3-3 (9)	34.69	> 47 mm
Mean value	34.50	> 48 mm

3. Experimental testing

3.3 Results and evaluation

The load–displacement relationship was plotted using Excel and presented as load–displacement diagrams. These diagrams were used to evaluate the stiffness of the beams and to compare the experimental results with those obtained from the simulation software. As previously mentioned, three different beam groups were tested in this study to investigate the influence of glass type on structural behavior.

- Beam Group 1 (float–float): These beams were made with two layers of float glass. They exhibited an approximately linear response up to the formation of the first visible crack in the glass web.
- Beam Group 2 (float–strengthened): These beams consisted of one layer of float glass and one layer of heat-strengthened glass. Similar to Group 1, they showed a linear response until the first crack appeared, primarily on the float glass side.
- Beam Group 3 (strengthened–strengthened): These beams were constructed with two layers of heat-strengthened glass. They maintained linear behavior throughout the entire loading process, up to the point of sudden and complete failure.

All tested beams exhibited a comparable bending response during the initial loading phase. The load–displacement relationship was approximately linear up to the formation of the first visible crack in the glass web. After this point, the behavior became non-linear due to stiffness degradation and the onset of fracture. The post-crack response and failure modes differed depending on the type of glass used in each beam group.

Across all groups, cracks initiated in the tension zone of the glass web, where tensile stresses were highest. This commonly led to fracture in the glass, and in some specimens, also contributed to localized failure in the timber flange on the tension side. Despite the formation of cracks, the composite beams retained partial load-bearing capacity due to the interaction between the glass, the PVB interlayer, and the timber components. As a result, complete structural collapse did not occur immediately, particularly in specimens with heat-strengthened glass. This highlights the role of lamination and material redundancy in improving post-crack performance.

In Group 1, which consisted of beams with double layers of float glass, the initial cracks appeared early in the loading process. The cracks formed symmetrically near the load application points and propagated gradually as loading increased. After the first crack, a clear reduction in global bending stiffness was observed, and the beams exhibited a more flexible response. Load-bearing was primarily sustained by the timber flanges following glass web fracture, and failure occurred progressively.

3. Experimental testing

In Group 2, each beam included one layer of float glass and one layer of heat-strengthened glass. The float glass began to crack under increasing load, but the presence of the heat-strengthened layer provided additional resistance. This resulted in a significantly higher load capacity compared to Group 1. Although global stiffness decreased slightly after float glass cracking, the reduction was modest, and the beams continued to carry increasing load until the sudden fracture of the heat-strengthened glass layer marked the final failure.

In Group 3, the beams were composed of two layers of heat-strengthened glass and demonstrated the highest load capacity among all groups. No visible cracks appeared prior to failure, and the global stiffness remained constant throughout the entire loading process. The load–displacement relationship was linear until both glass layers fractured simultaneously, resulting in a sudden and brittle failure without prior warning.

The raw data exported from the testing machine were carefully analyzed, and the corresponding load–displacement graphs were generated. As described in Section 2.2, the bending stiffness of each specimen was evaluated based on the linear portion of the load–displacement curve. The calculated bending stiffness values for each beam group are summarized in Table 10.

Table 10: Calculated bending stiffness of each group.

	Specimen (Sample number)	EI from global displacement (initial linear range) (MNm ²)	EI from local displacement (MNm ²)
Beam group 1	1-1 (1)	0.954	1.035
	1-2 (2)	0.901	1.009
	1-3 (3)	0.907	1.007
	Mean value	0.920	1.017
Beam group 2	2-1 (4)	0.898	0.957
	2-2 (5)	0.897	0.976
	2-3 (6)	0.919	1.019
	Mean value	0.904	0.984
Beam group 3	3-1 (7)	0.922	1.025
	3-2 (8)	0.863	0.925
	3-3 (9)	0.884	0.969
	Mean value	0.889	0.973

4. Analytical solution

4.1 Analytical method

Analytical Method Timber–glass composite beams are structural elements composed of materials with differing mechanical properties. Typically, timber flanges are bonded to a central glass web using a silicone adhesive. This adhesive interface plays a critical role in transferring shear forces between the components, but due to its relatively low stiffness, only partial composite action occurs. As a result, classical bending theory, which assumes full interaction between components, is not directly applicable.

To account for this behavior, the gamma-method is used. It introduces a correction factor γ for the moment of inertia, enabling more accurate prediction of deflections and stresses by considering shear deformation, also referred to as shear lag, in the adhesive and interface zones. The gamma-method is derived from Timoshenko beam theory, which incorporates both bending and shear deformations. It is particularly suited for layered composite beams, such as timber–glass systems, where flexible bonding interfaces lead to partial interaction under load.

Figure 25 presents the cross-sectional geometry of the composite beam, including all relevant dimensions and notation used in the following analytical expressions.

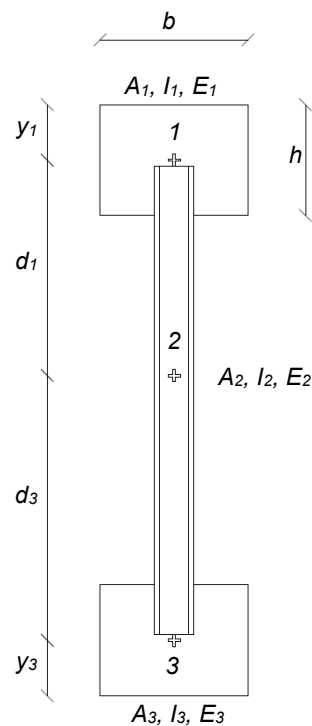


Figure 25: Cross-section and geometric properties of the composite timber-glass beam.

4. Analytical solution

Normal Stress in Bending:

The normal stress in a homogeneous beam section under bending is given by:

$$\sigma_{bend} = \frac{My_c}{I} \quad (4.1)$$

where:

M = the internal bending moment at the section's axis

y_c = the perpendicular distance from the neutral axis to a point on the section

I = the moment of inertia of the section

In composite timber-glass beams, the section of the beam consists of material 1 with elastic modulus E_1 , material 2 with elastic modulus E_2 , and material 3 with elastic modulus E_3 .

To apply this to a composite beam, each component must be transformed into an equivalent material using a modular ratio n_i , defined as:

$$n_i = \frac{E_i}{E_r}$$

E_i = modulus of elasticity for material i

E_r = reference modulus of elasticity (generally smaller E)

Regarding differences in modulus of elasticity, Equation can be defined as:

$$\sigma_{bend} = \frac{My_c}{I} n_i \quad (4.2)$$

Application of the Gamma-Method:

Due to the shear deformation in the adhesive layer, full interaction between glass and timber cannot be assumed. The gamma-method introduces a reduction factor γ that adjusts the stiffness and stress distribution to reflect partial composite action. By replacing γ the corrected stress formulas become:

4. Analytical solution

- Stress in the center of mass in flange:

$$\sigma_{bend_cent} = \frac{M y_c}{I_{eff}} \gamma n_i \quad (4.3)$$

- Stress in the wooden flange:

$$\sigma_{bend_cent} = \frac{M}{I_{eff}} (\gamma y_c + y_f) n_i \quad (4.4)$$

- Stress in the glass web:

$$\sigma_{bend_cent} = \frac{M}{I_{eff}} \frac{h_{web}}{2} \quad (4.5)$$

where:

I_{eff} = effective moment of inertia

γ = reduction factor

y_f = the position of the neutral axis

Effective Moment of Inertia:

The effective moment of inertia I_{eff} , considering partial interaction through the gamma factor, is given by:

$$I_{eff} = \sum_i \frac{1}{12} n_i b_i h_i^3 + n_i A_i d_i^2 \quad (4.6)$$

Reduction Factor γ :

Möhler [27] introduced the reduction factor γ which can be calculated as:

$$\gamma = \frac{1}{1 + \frac{\pi^2 E A_i}{L^2 K_k}} \quad (4.7)$$

where

L is the length of the beam

K_k is the stiffness of connection, given by:

$$K_k = \frac{2Gh_{fg}}{t_1} + \frac{Gw_{fg}}{t_2} \quad (4.8)$$

4. Analytical solution

Neutral Axis Position:

The vertical position of the neutral axis is y_f and can be found as formula below:

$$y_f = \frac{\sum_i n_i A_i \bar{y}_i}{\sum_i n_i A_i} \quad (4.9)$$

where:

A_i area of cross sections

d_i , b_i and h_i are geometric properties of each section, see Figure 25.

4.2 Analytical results

The analytical expressions presented in this chapter were used to evaluate the behavior of the timber–glass composite beam subjected to four-point bending. Based on the gamma-method described in Equations (4.3)–(4.9), the effective bending stiffness of the composite section was determined to be approximately $EI = 1.02 \text{ MNm}^2$.

Using the four-point bending displacement relationship given in Equation (2.7), the theoretical load of the beam was calculated. The theoretical total force was approximately 38.9 kN.

5. Simulation in Abaqus

5.1 Introduction

The finite element method (FEM) is a widely used numerical approach for analyzing complex structural systems composed of different materials and geometries. It works by dividing large structures into smaller, simpler components (finite elements), which together form a mesh that can be solved computationally. Various commercial FEM tools are available to support such analyses.

In this study, the finite element software Abaqus was used to simulate the behavior of the timber–glass composite beams. Abaqus allows the modeling of composite structures and provides robust capabilities for simulating elastic deformation, contact conditions, and multi-material assemblies [24].

Due to the limitations in modeling multiple glass types in a single simulation, and since the primary goal was to evaluate the initial bending stiffness EI in the elastic range before crack initiation, only one representative simulation was performed. Previous studies have shown that composite action affects the bending stiffness of timber–glass beams [5, 6, 11]. Therefore, one representative simulation was considered sufficient for this part of the study.

This simulation focuses solely on the evaluation of bending stiffness and does not include the effects of cracking, fracture, or post-crack behavior, which are more material-specific and would require nonlinear fracture mechanics or cohesive zone modeling beyond the scope of this study.

5.2 Modelling

To simulate the four-point bending test of the composite beams, only one representative beam was modeled in Abaqus. This simplification was chosen because, in the linear elastic range (prior to cracking), all tested beam types exhibit comparable structural behavior. Therefore, one simulation was sufficient for evaluating the elastic bending stiffness.

Due to the symmetric geometry and loading conditions, only half of the beam length (2400 mm) was modeled to reduce analysis time. The timber flanges and the glass web were modeled as separate parts and assembled together using a 2 mm silicone layer representing the adhesive interface. The glass web was modeled as a laminated structure consisting of two outer glass layers and a 1 mm-thick PVB interlayer.

5. Simulation in Abaqus

To distribute the applied load and prevent local stress concentrations, steel plates (60×60 mm, 8 mm thick) were introduced at the loading and support positions. The boundary conditions were defined such that vertical movement (along the y -axis) was restricted at the supports. At the load application points, the beam was only allowed to move vertically.

The simulation was performed under displacement-controlled loading, with a prescribed displacement of 1 mm applied at the load points. This value was selected because the beam behavior in the elastic range is linear. The resulting reaction forces were extracted after several time steps, allowing the calculation of the corresponding applied loads and evaluation of the effective bending stiffness.

A schematic model setup, including the load and support configuration, coordinate system, and model symmetry, is shown in Figure 26.

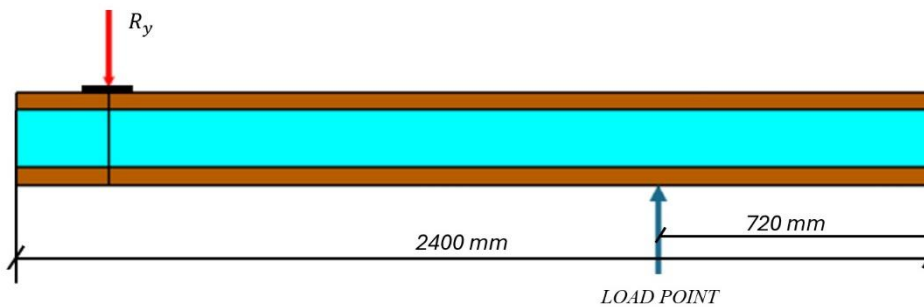


Figure 26: Model configuration and boundary conditions.

5.3 Material definition

All materials were defined separately. As mentioned in Section 2.1.3, the timber flanges were made of LVL Kerto, and the material properties were defined as orthotropic and linear elastic in Abaqus. Simplified transverse elastic modulus values of $E_2 = E_3 = 1$ GPa were used in the model. The elastic moduli and shear moduli G_{ij} used in the model are presented in Table 11.

Table 11: Material properties used for the LVL Kerto wood in the Abaqus simulation.

E_1 (GPa)	E_2 (GPa)	E_3 (GPa)	G_{12} (GPa)	G_{13} (GPa)	G_{23} (GPa)
13.8	1	1	600	380	50

5. Simulation in Abaqus

For glass web, the material properties were defined as isotropic and linear elastic in Abaqus.

As mentioned in Section 2.1.4, Silicone SG-500 adhesive was used to connect the wooden flanges and glass web and was also modeled as an isotropic and linear elastic material.

The PVB layer between the glasses and steel plate were modeled separately with isotropic and linear elastic properties.

The elastic modulus E and Poisson's ratio ν used for these materials are presented in Table 12.

Table 12: Material properties used in the Abaqus simulation.

Material	Elastic modulus E (MPa)	Poisson's ratio ν
Glass	70000	0.23
Silicone SG-500	3.17	0.46
PVB film	2	0.45
Steel	210	0.3

5.4 Mesh and Supports

The geometry of the beam is uniform along its entire length, allowing for a regular mesh to be applied. A structured rectangular mesh with an approximate element size of 10 mm was used for the timber flanges and glass layers. For the silicone adhesive, a finer mesh of 2 mm was applied to capture deformation more accurately, while the steel plates at the supports were meshed with 5 mm elements. This ensured accurate stress distribution and compatibility at all interfaces.

The support conditions were defined according to the experimental setup. At the left end of the beam, a simple support was modeled in Abaqus by constraining the vertical displacement, while horizontal translation and rotation were left free. This replicates the physical behavior of a pinned support. The right end of the model was defined as a symmetry boundary, since only half of the beam was modeled (2400 mm) to reduce analysis time. The support conditions and loading configuration are illustrated later in Figure 28.

5. Simulation in Abaqus

5.5 Results

As mentioned before, the experimental test was performed under displacement-controlled loading, and the corresponding load was extracted from the test machine. Global and local displacement were measured using two displacement sensors

Since the behavior is assumed to be linear until first failure of the glass, in the simulation the beam deflection was limited to only 1 mm at the load point. The corresponding reaction force at the load point was eventually taken from the results.

The benefit of using Abaqus for this numerical study is that the deflection of any point needed can easily be measured. Therefore, deflection at the middle point of the beam and load point could be read directly, and from this, the local displacement in the middle of the beam was determined. Figure 27 shows the deformed beam from Abaqus.

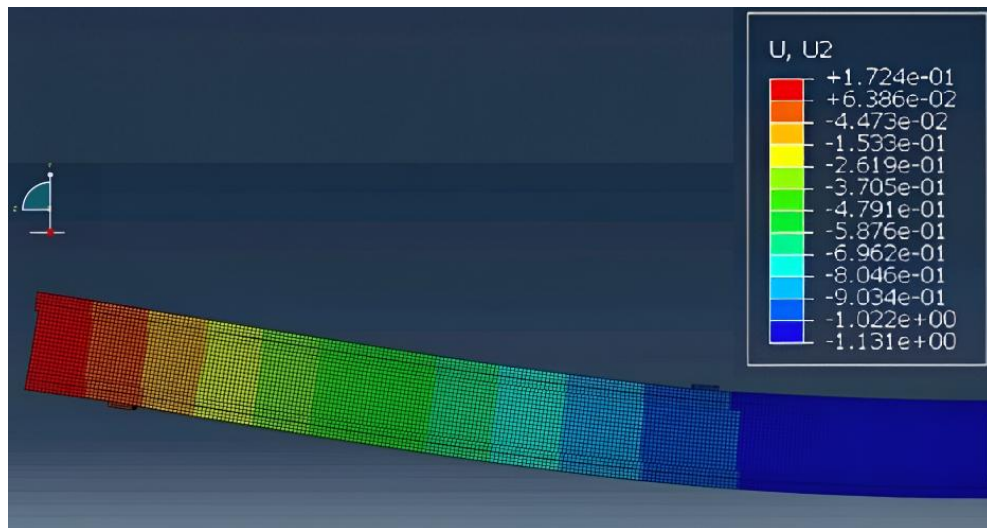


Figure 27: Deformed shape of the simulated half beam (deformation visually scaled for clarity).

From the results, displacement was measured at three key locations along the beam, as shown in Figure 28:

1. Middle of the beam (global displacement) – to record the overall deflection response.
2. At a distance of $2.5h$ from the midspan (local displacement) – to capture localized deformation in the composite zone.
3. At the load application point – to monitor deflection directly under the applied force.

5. Simulation in Abaqus

- 1 - midspan point (global displacement)
- 2 - local displacement point
- 3 - load point
- 4 - support condition

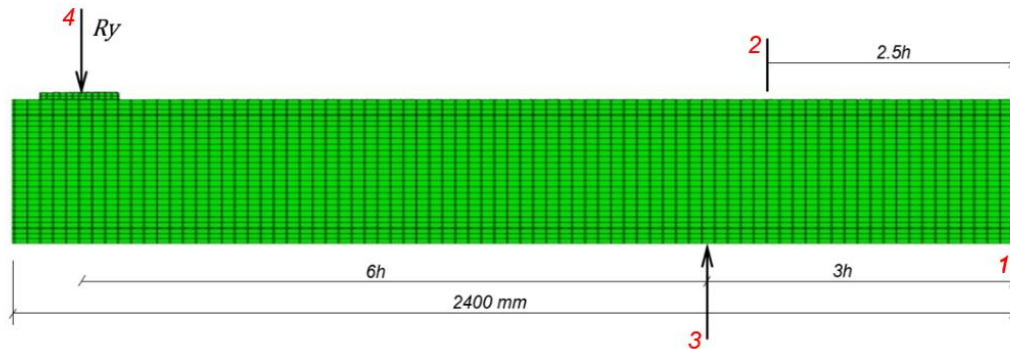


Figure 28: Measurement positions and support condition used in the Abaqus model.

The displacement and corresponding loads extracted from Abaqus is shown in Table 13.

Table 13: Results from Abaqus.

Double heat-strength glass beam	Displacement at load point (mm)	Global displacement (mm)	Corresponding total force (kN)	Max tension stress (MPa)		
				glass	wood flange (outside)	wood flange (inside)
1		1.127	0.713	2.2	0.7	0.6

Table 14 presents a comparison of the maximum tensile stress obtained from the experimental test, Abaqus simulation, and analytical calculation. The comparison was used to evaluate the agreement between the different methods.

Table 14: Comparison of maximum tensile stress in the composite beam.

Beam Specimens	Max tension stress from experimental test (MPa)	Max tension stress from Abaqus (MPa)	Max tension stress from analytical formula (MPa)
Double heat-strength glass	2.135	2.201	2.213

5. Simulation in Abaqus

The Abaqus simulations were performed using a displacement-controlled loading approach. In the simulation, a vertical displacement of 1 mm was applied at the load point, corresponding to the beam's linear-elastic response. The corresponding reaction force and displacement values obtained from the simulation were then used to calculate the bending stiffness EI using the standard formulas for four-point bending relationship described in Section 2.2. This approach enabled comparison with the analytical and experimental results under the same loading conditions.

Table 15 presents the calculated bending stiffness values based on the Abaqus simulation results.

Table 15: Calculated bending stiffness values from Abaqus simulation results using the four-point bending relationships.

Beam Specimens	EI from displacement at load point (MNm ²)	EI from global displacement (MNm ²)	EI from local displacement (MNm ²)
Double heat-strength glass	0.347	0.221	0.024

6. Analysis

6.1 Load-bearing capacity

In this section, the results from the experimental tests, analytical calculations, and Abaqus simulations are presented and compared. The analytical and numerical calculations were evaluated based on a vertical displacement of 1 mm at the load application point.

- The maximum total force before failure for the double heat-strength glass specimen (specimen 3-1) was obtained from the load–displacement curve and was equal to 36.05 kN, as shown in Table 9.
- The analytical total force (38.9 kN) was calculated using the bending stiffness $EI= 0.954$ (from Table 10) and the standard equation for four-point bending (see Section 2.7), rearranged to solve for the total force:

$$P = \frac{v_{load.p} * 6EI}{a^2(3L - 4a)}$$

- The total force from Abaqus was determined from the reaction force obtained in the linear simulation. A reaction force of 0.713 kN corresponded to a vertical displacement of 1 mm in the simulated half beam, as presented in Table 13. Assuming linear-elastic behavior, the force–displacement relationship was extended to the experimental displacement level of approximately 47 mm, resulting in an estimated total force of about 33.5 kN for the full beam. The lower value compared to the experimental result (36.05 kN) reflects the limitations of the linear Abaqus model, which does not include cracking, nonlinear deformation, or post-fracture behavior observed in the experimental test.

The results obtained from the laboratory tests were compared with those from the Abaqus simulations and the analytical gamma-method calculations. Table 16 summarizes this comparison and shows the agreement between the three approaches.

Table 16: Comparison results from experimental test, Abaqus and analytical solution.

Beam Specimens	Total force from experimental test (kN)	Total force from Abaqus (kN)	Total force from analytical solution (kN)
Double heat-strength glass	36.05	33.50	38.90

6. Analysis

The comparison shows that the experimental results are slightly higher than both the analytical and numerical predictions. This difference can be attributed to nonlinear effects and post-fracture behavior of the glass, which are not included in the linear Abaqus model.

6.2 Bending stiffness comparison

The bending stiffness values obtained from Abaqus simulations are significantly lower than those from the experimental tests, with differences of approximately 75% for global displacement and 98% for local displacement. This discrepancy arises mainly because the experimental results were recorded at much higher displacement levels (around 47 mm), capturing nonlinear behavior such as cracking, local damage, and post-fracture resistance. In contrast, the Abaqus simulations were performed within the linear-elastic range at a small displacement of 1 mm, before any cracking or nonlinear effects occurred. These findings highlight the importance of evaluating stiffness under realistic deformation conditions.

It should also be noted that the global stiffness values are lower than the local stiffness values. This is because the global displacement includes deformation from the whole beam, while the local displacement is measured only in the middle part of the beam. Therefore, the local stiffness values become higher. A comparison of all results is presented in Table 17.

Table 17: Comparison results from experimental test and Abaqus.

Beam Specimens	<i>EI</i> from global displacement (MNm ²)		<i>EI</i> from local displacement (MNm ²)	
	Experimental test	Abaqus	Experimental test	Abaqus
Double heat-strength glass	0.89	0.22	0.97	0.02

7. Conclusions

The purpose of this study was to investigate timber–glass composite beams and their behavior under bending load, as well as to calculate the stiffness of the composite timber–glass beams. Similar work has been done earlier, unique in this study is the use of laminated glass for the web. Additionally, different combinations of glass types were used for the webs.

By comparing all results from the experimental tests, the analytical solution, and finite elements simulations, the following can be concluded:

- For all groups of beams, three repetitions were experimentally tested. Each group showed similar results so that the results for each group are considered trustworthy.
- The FEM simulations did not fully match the experimental results because the Abaqus model was limited to linear behavior. However, the simulations still gave useful information about the stiffness of the beams and can be used to study other beam geometries.
- Composite timber–glass beams from all three groups, namely (1) double float glass, (2) double heat-strengthened glass, and (3) one layer of float glass combined with one layer of heat-strengthened glass, demonstrated adequate strength and load-bearing capacity under four-point bending tests. The results showed that all configurations maintained structural integrity during the tests, and their performance under service-level displacements aligned well with the analytical predictions.
- Based on the results, it can be confirmed that the beams have lower durability in the tension zone. Cracks in the glass webs consistently initiated in the tension zone first, which subsequently led to the failure of the timber flange in that region. When the critical tensile stress was reached, cracks appeared; however, the elements including double heat-strengthened glass retained partial load-bearing capacity after initial cracking. This observation suggests that the glass web did not completely shatter but exhibited softened bending stiffness, particularly in beams with double heat-strengthened glass, allowing the structure to maintain some residual performance after damage.
- Beams made by heat-strength glass show higher load bearing capacity in comparison to beams that are made by float-glass only.
- The experimental results showed good reproducibility for all beam groups, indicating that the type of glass had only a limited effect on the bending stiffness.

7. Conclusions

The effects of temperature, dynamic loads, creep and the effects of sudden shocks on beams and glass, were not considered in this study. Therefore, it is highly recommended that aspects should be analyzed for future studies. It is also possible to use different adhesives with different stiffness to determine the effect on the stiffness of the beams using adhesives with a higher stiffness will probably reduce shear I_a , the gamma value will increase and hence will bending stiffness. This issue is important from the point of view of the long-term stability of beams.

Appendix

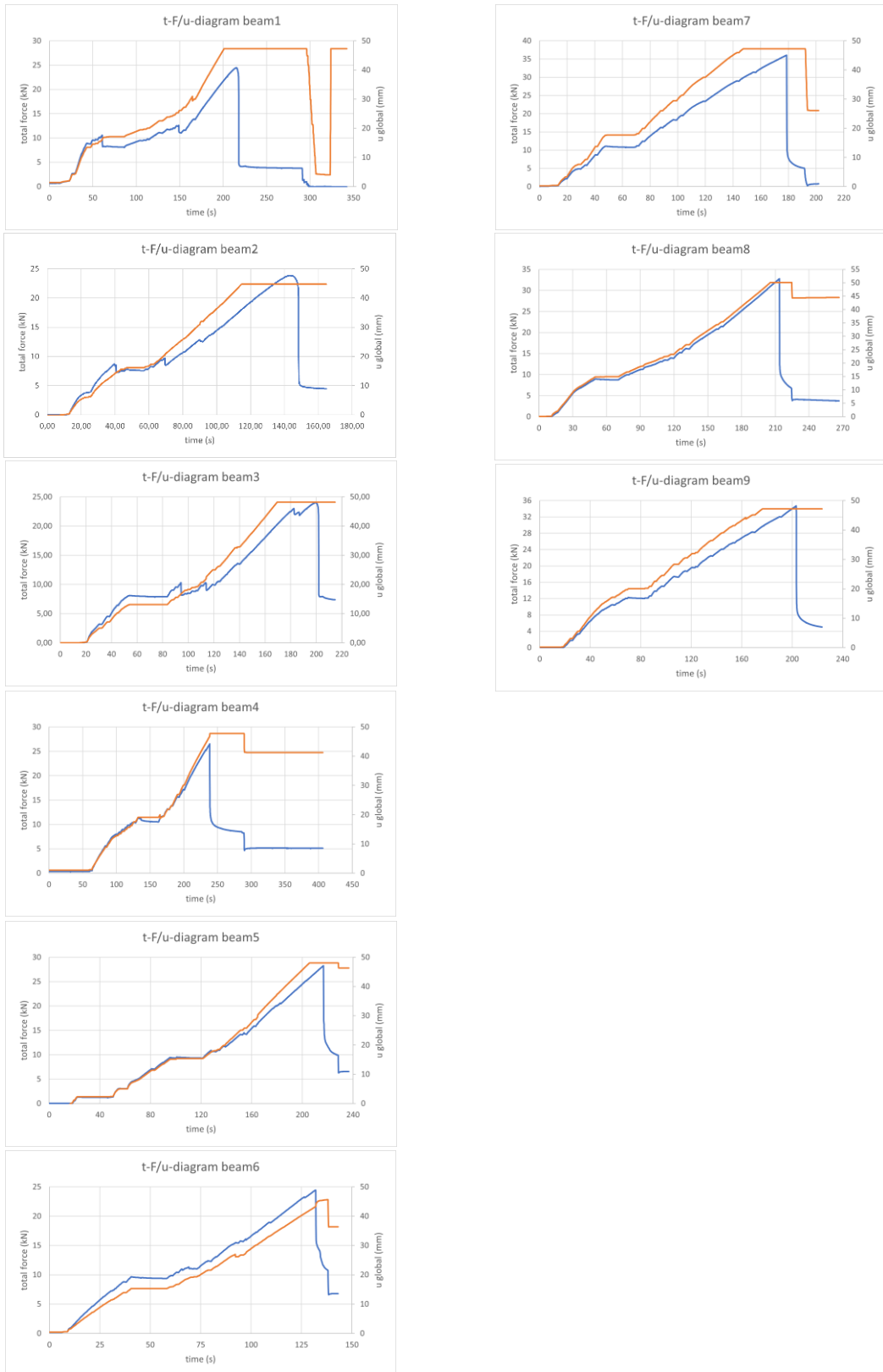


Figure 29: Load-time and time-global displacement diagram.

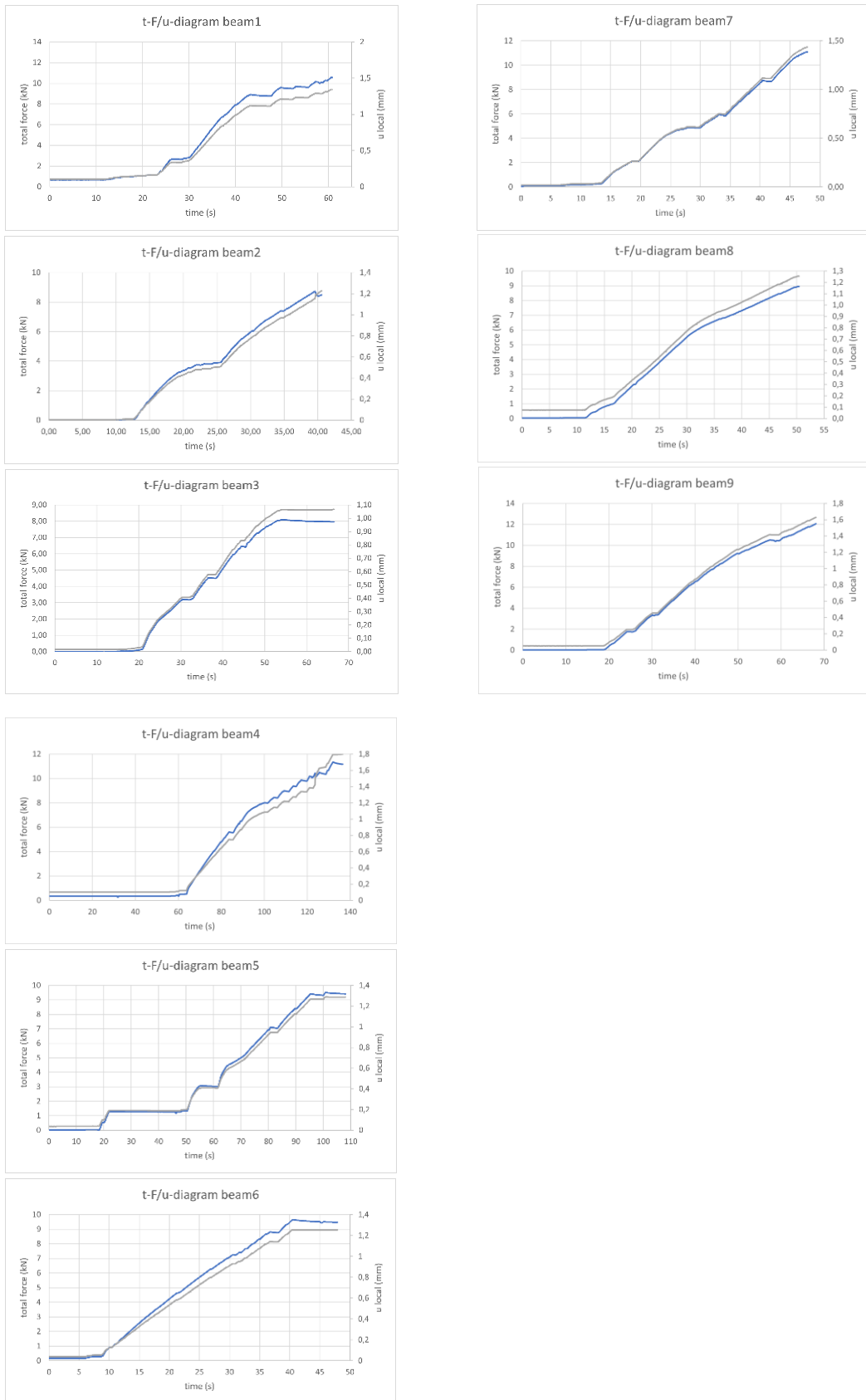


Figure 30: Load-time and time-local displacement diagram.

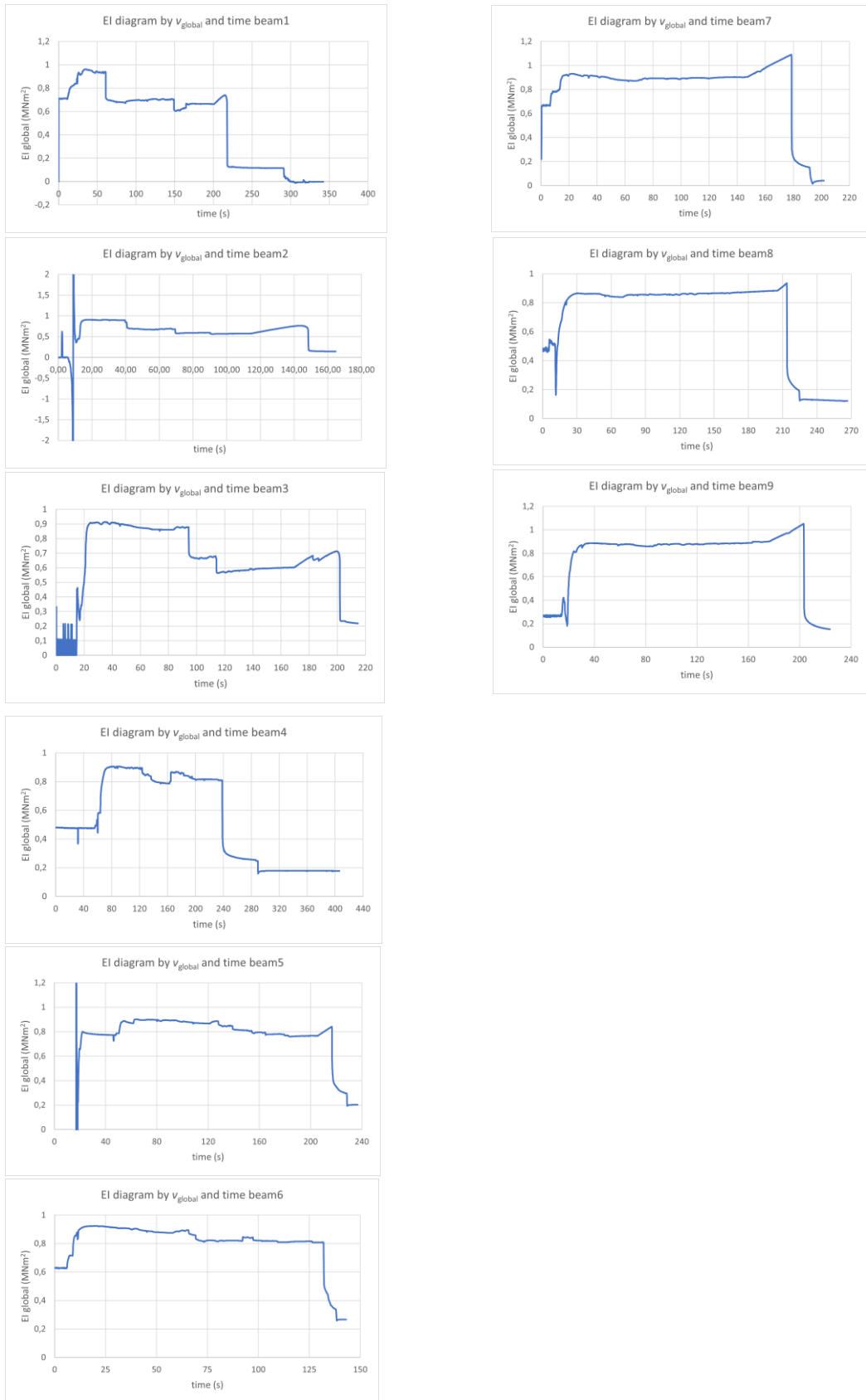


Figure 31: Bending stiffness diagram from global displacement.

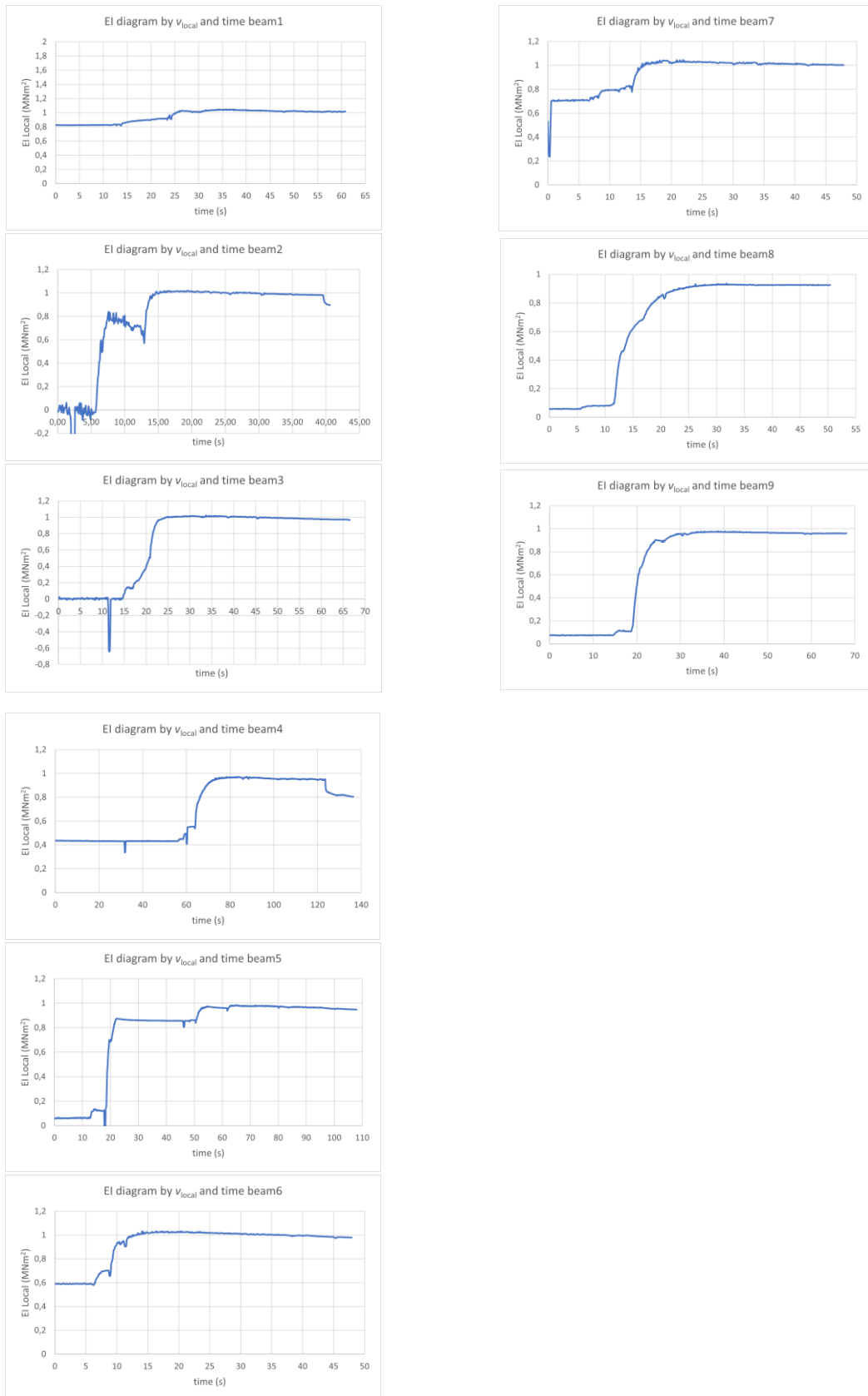


Figure 32: Bending stiffness diagram from local displacement.

References

- [1] R. Klos, C. Bedon, "Recent developments in structural glass applications: A review," *Journal of Building Engineering*, vol. 29, 101135, 2020.
- [2] J. Hamm, "Tragverhalten von Holz und Holzwerkstoffen im statischen Verbund mit Glas," EPFL, Lausanne, 2000.
- [3] K. Kreher, "Tragverhalten und Bemessung von Holz-Glas-Verbundträgern unter Berücksichtigung der Eigenspannungen im Glas," EPFL, Lausanne, 2004.
- [4] J. Natterer, K. Kreher, J. Natterer, "New joining techniques for modern architecture," *Rosenheimer Fenstertage Conference*, Rosenheim, Germany, 2002.
- [5] M. Kozłowski, M. Kadela, J. Hulimka, "Numerical investigation of structural behaviour of timber–glass composite beams," *Procedia Engineering*, vol. 161, pp. 990-1000, 2016.
- [6] L. Blyberg, E. Serrano, "Timber–glass adhesively bonded I-beams: Experimental and numerical investigations," *Glass Performance Days*, Tampere, Finland, 2011.
- [7] L. Blyberg, E. Serrano, "Design approaches for timber–glass beams," *Proceedings of the International at Glasstec*, Düsseldorf, Germany, 2014.
- [8] V. Rajčić, N. Perković, D. Damjanović, J. Barbalić, "Influence of friction on the behavior and performance of prefabricated timber–bearing glass composite systems," *Sustainability*, vol. 14, no. 3, p. 1102, 2022.
- [9] P. Cruz, J. Pequeno, "Timber–glass composite beams: Mechanical behaviour and architectural solutions," *Challenging Glass Conference*, Delft University of Technology, Netherlands, 2008.
- [10] P. Cruz, J. Pequeno, "Timber–glass composite structures: Mechanical behaviour and applications," *World Conference on Timber Engineering WCTE*, Riva del Garda, Italy, 2010.
- [11] P. Cruz, J. Pequeno, "Timber–glass composite structures: Adhesive behaviour and structural performance," *International Journal of Architectural Engineering and Design*, vol. 7, no. 2, pp. 45-56, 2011.
- [12] P. Cruz, J. Pequeno, "Timber–glass structures: Experimental and numerical studies on adhesive bonding and structural response," *Construction and Building Materials*, vol. 47, pp. 240-250, 2013.
- [13] M. Premrov, M. Zlatinek, A. Štrukelj, "Experimental analysis of load-bearing timber–glass I-beam," *Construction of Unique Buildings and Structures*, vol. 4, no. 19, pp. 11-20, 2014.
- [14] M. Držičnik, A. Štrukelj, M. Premrov, "Influence of the bonding boundary conditions of timber–glass I-beams on load-bearing capacity and stiffness," *Applied Sciences*, vol. 12, no. 4, p. 1770, 2022.

References

- [15] K. Rodacki, K. Furtak, "Numerical analysis of crack development of timber–glass composite I-beams in the extended finite element method (XFEM)," *Composite Structures*, vol. 209, pp. 349-361, 2019.
- [16] H. A. A. Buyuktaskin, M. S. Yatagan, G. E. Soyoz, L. Tanacan, M. Dilmaghani, "Experimental investigation of the durability of load-bearing timber–glass composites under the effects of accelerated aging," *Journal of Green Building*, vol. 14, no. 2, pp. 45-59, 2019.
- [17] Ž. Unuk, A. Štrukelj, V. Ž. Leskovar, M. Premrov, "Novel composite connection for timber–glass composite structures," *Archives of Civil and Mechanical Engineering*, vol. 20, no. 1, pp. 1-6, 2020.
- [18] L. Gemi, E. Madenci, Y. O. Özkılıç, "Experimental, analytical and numerical investigation of pultruded GFRP composite beams infilled with hybrid FRP reinforced concrete," *Engineering Structures*, vol. 244, p. 112790, 2021.
- [19] S. Ebnesajjad, *Adhesives Technology Handbook*, 2nd ed., William Andrew Publishing, 2008.
- [20] Wesbeam, "A closer look at the LVL manufacturing process," 2023. [Online]. Available: <https://wesbeam.com/resources/articles/blog/january-2023/a-closer-look-at-the-lvl-manufacturing-process>. [Accessed March 21, 2025].
- [21] Oklahoma State University Extension, "Laminated veneer lumber (LVL) as a construction material," [Online]. Available: <https://extension.okstate.edu/fact-sheets/laminated-veneer-lumber-lvl-as-a-construction-material.html>. [Accessed March 21, 2025].
- [22] E. M. Petrie, *Handbook of Adhesives and Sealants*, 2nd ed., McGraw-Hill Professional, 2007.
- [23] J. M. Gere, B. J. Goodno, *Mechanics of Materials*, 8th ed., Cengage Learning, 2012.
- [24] Dassault Systèmes, "Abaqus 6.14 Documentation," Dassault Systèmes Simulia Corp., Providence, RI, 2014.
- [25] VTT Technical Research Centre of Finland, "Technical Approval for LVL (Kerto) by Metsä Wood (Certificate No. 184/03)," 2012.
- [26] N. N. Greenwood, A. Earnshaw, *Chemistry of the Elements*, 2nd ed., Butterworth-Heinemann, 1997.
- [27] K. Möhler, "Über das Verhalten von Biegeträgern und Druckstäben mit zusammengesetzten Querschnitten und nachgiebigen Verbindungsmitteln," Universität Karlsruhe, Karlsruhe, 1956.
- [28] L. Imanizabayo and O. Mohammadianfar, "Study of the Bonding Properties for Timber–Glass Composite Beams: The influence of viscoelastic adhesives on the load-bearing capacity," Master's Thesis, Linnaeus University, Växjö, Sweden, 2015.

Lnu.se

Faculty of Technology

351 95 Växjö, Sweden

Telephone: +46 772-28 80 00, fax +46 470-832 17